# Differential Proton-Proton Scattering Cross Section for energies between 1.9 MeV and 50 MeV

Marcus Moser

Universität der Bundeswehr München

HOCHSCHULE FÜR ANGEWANDTE WISSENSCHAFTEN·FH MÜNCHEN

München 2011

# Differential Proton-Proton Scattering Cross Section for energies between 1.9 MeV and 50 MeV

Marcus Moser

## MASTER - THESIS

Hochschule München

vorgelegt von

Marcus Moser

aus Bad Aibling

Betreuer: Dr. Patrick Reichart

Erstgutachter: Prof. Dr. Stefan Sotier

Zweitgutachter: Prof. Dr. Günther Dollinger

Tag der Abgabe: 11.02.2011

# Contents

# ABSTRACT

We present a phase shift analysis of differential elastic proton-proton scattering cross sections $(\mathrm{d}\sigma/\mathrm{d}\Omega)_{\mathrm{pp}}$ in the energy range from 1.9 MeV to 50 MeV and laboratory scattering angles $\theta_{\mathrm{lab}} = 15 \ldots 75$. It results in an accurate representation of the experimental data by an analytical function for $(\mathrm{d}\sigma/\mathrm{d}\Omega)_{\mathrm{pp}}(E, \theta)$. The average statistical error of the resulting data fit is 0.2%. For a fast evaluation we extract an $[\boldsymbol{E}, \theta]$-matrix for $(\mathrm{d}\sigma/\mathrm{d}\Omega)_{\mathrm{pp}}$ with a negligible interpolation error smaller than 0.02%. This data may be relevant for data evaluation for hydrogen analysis when using proton-proton scattering.

# Chapter 1

# INTRODUCTION

Elastic proton-proton scattering (pp-scattering) at MeV energies has proven to be the most sensitive method for hydrogen depth profiling at micrometer depth resolution. Even a detection limit as low as $0.08\,\text{ppm}$ was achieved in diamond material utilizing a detector setup covering $\Omega = 2.4\,\text{sr}$ of solid angle (1). In particular, the high sensitivity allows this method to be applied to proton micro-probes in order to image hydrogen distributions with micrometer or better lateral resolution, resulting in a 3D hydrogen microscopy tool (1). Beside the high sensitivity there is another main advantage compared to other methods for hydrogen imaging like IR-microscopy or imaging SIMS (secondary ion mass spectrometry): There is no need of reference standards to calibrate the detection cross section or absorption coefficient for matrix or other material/sample dependent effects. This universal application potential is due to the high proton energy that is 5-6 orders of magnitudes larger than the binding energy of the hydrogen atoms and hence the chemical and structural environment has negligible influence on the differential proton-proton scattering cross section and thus the detection rate.

The hydrogen areal density $n_{\text{H}}\Delta z$ in at/cm$^2$, which is the product of the hydrogen density $n_{\text{H}}$ and the sample thickness $\Delta z$ in a certain depth $z$ of the sample,

can be calculated by (2)

$$n_\mathrm{H}\Delta z = \frac{N_\mathrm{pp}}{N_0 \cdot \sigma_\mathrm{pp}} \ \text{ with } \ \sigma_\mathrm{pp} = \int\limits_{\Omega_\mathrm{pp}} \int\limits_{\Delta z} \left(\frac{\mathrm{d}\sigma}{\mathrm{d}\Omega}\right)_\mathrm{pp} \varepsilon_\mathrm{pp}(z)\mathrm{d}z\mathrm{d}\Omega \qquad (1.1)$$

with $N_\mathrm{pp}$ being the number of detected pp-scattering events, $N_0$ is the number of incident protons, $\varepsilon_\mathrm{pp}(z)$ accounts for the detection efficiency within the solid angle of detection $\Omega_\mathrm{pp}$ and $(\mathrm{d}\sigma/\mathrm{d}\Omega)_\mathrm{pp}$ is the differential pp-scattering cross section. It varies with depth $z$ due to the change of the proton energy $E$ from energy loss in the sample before the scattering event happens. The accuracy of incident beam current measurment $(N_0)$ is mainly affecting the total accuray and is a critcal experimental task, but as long as particle statistics is good enough and the solid angle is well defined the accuracy in hydrogen analysis is mainly given by the accuracy of $(\mathrm{d}\sigma/\mathrm{d}\Omega)_\mathrm{pp}$. The aim of this paper is to extract $(\mathrm{d}\sigma/\mathrm{d}\Omega)_\mathrm{pp}$ from experimental data found in literature for a wide range of scattering angles $\theta$ and incident proton energies $E$ with optimum accuracy.

Existing databases (see Section 3.1) give data sets in discrete steps. With the aim of a closed nuclear potential theory, partial-wave analyses of this data have been performed for a broad energy range up to $E = 450\,\mathrm{MeV}$ (e. g.(3; 4; 5)). These analyses result in a parameterization of the nuclear potential with many parameters additionally to nuclear phase shifts. We found this to be a too complex evaluation method for $(\mathrm{d}\sigma/\mathrm{d}\Omega)_\mathrm{pp}$ for applied nuclear physics in the range of usable energies from $1.9\ldots50\,\mathrm{MeV}$. We focus here on this energy range and an angular range of $\theta_\mathrm{lab} = 15°\ldots75°$ that is the maximum reasonable range used for hydrogen analysis by proton-proton scattering. Lower energies or steeper angles reduce the analysable sample thickness to uncomfortably low values and higher energies are difficult to analyse with reasonable detector effort. With this restriction, we have developed two new kinds of parameterizations of $(\mathrm{d}\sigma/\mathrm{d}\Omega)_\mathrm{pp}$:

**(A)** A simple exponential approximation with an analytical formula that can

be applied without numerical calculations, but with errors up to $4\,\%$, and hence slightly larger than the experimental errors at large angles and some particular data sets. Errors are within the experimental uncertainties ($\sim 1\%$) for a limited range of angles and energies. This parameterization is already published in (2), but for completeness and some critical typos in the book chapter we summarize the results of the parameterization with the revision of the former publication and we additionally present the validation of the fit.

**(B)** An approximation using physical functions, which describes a series expansion of $(\mathrm{d}\sigma/\mathrm{d}\Omega)_{\mathrm{pp}}$ in the angular momenta with nuclear phase shifts as parameters, similar to the above mentioned theoretical nuclear potential analyses, but with as low as possible parameters. The statistical error of this fit is even less than the given experimental errors due to the large number of simultaneously fitted data.

# Chapter 2

# THEORY

## 2.1  NUCLEON-NUCLEON SCATTERING

Proton-proton scattering is scattering of two identical particles (e. g. (6; 7)). Due to indistinguishability of two scattered protons at angles $\theta_{\mathrm{CM}}$ and $\pi - \theta_{\mathrm{CM}}$ in the center-of-mass (CM) system, it comes to an interference phenomenon. The scattering amplitudes $f(\theta_{\mathrm{CM}})$ and $f(\pi - \theta_{\mathrm{CM}})$ have to be added for both particles when considering the exchange symmetry (8)

$$f_J(\theta) = f(\theta_{\mathrm{CM}}) + (-1)^J f(\pi - \theta_{\mathrm{CM}}) \tag{2.1}$$

for each state of total spin $J$. If scattering is independent of the spin $s$ of the particles (no spin flip), and no spin polarization occurs, Eq. (2.1) has to be weighted with the statistical spin states in order to obtain the differential pp-scattering cross section

$$\frac{d\sigma}{d\Omega} = \sum_{J=0}^{2s} \frac{2J+1}{(2s+1)^2} |f_J(\theta_{\mathrm{CM}})|^2 \tag{2.2}$$

with the spin $s$ for the particle.

For scattering on the Coulomb potential only, Eq. (2.2) results in the well known

Mott scattering cross section (8) that is given for the CM system by

$$\left(\frac{d\sigma}{d\Omega}\right)_{\text{Mott}} = \frac{\eta^2}{4k^2}\left[\sin^{-4}\frac{\theta_{\text{CM}}}{2} + \cos^{-4}\frac{\theta_{\text{CM}}}{2} + \frac{(-1)^{2s}}{2s+1}\frac{2\cos(\eta\ln(\tan^2\frac{\theta_{\text{CM}}}{2}))}{\sin^2\frac{\theta_{\text{CM}}}{2}\cos^2\frac{\theta_{\text{CM}}}{2}}\right] \quad (2.3)$$

$$\text{with } k = \frac{m_{\text{p}}v}{2\hbar}$$

$$\eta = \frac{e^2}{4\pi\epsilon_0 v\hbar} \text{ Sommerfeld - parameter}$$

with $m_{\text{p}}$ being the proton mass, $v$ the relative velocity, $e$ the electronic charge, $\hbar = \frac{h}{2\pi}$ the Planck constant divided $2\pi$ and $\epsilon_0$ the dielectric constant. The first coefficient can be written for the calculations in the CM-system

$$\frac{\eta^2}{4k^2} = \left(\frac{e^2}{4\pi\epsilon_0 m_{\text{p}}v^2}\right)^2 = \left(\frac{e^2}{4\pi\epsilon_0 2m_{\text{p}}^*v^2}\right)^2 = \left(\frac{e^2}{4\pi\epsilon_0 4E_{\text{CM}}}\right)^2 \quad (2.4)$$

with $m_{\text{p}}^* = m_{\text{p}}/2$ the reduced proton mass and $E_{\text{CM}}$ for the kinetic energy in the CM-system.

For the relativistic transformation of the kinetic energy $E_{\text{CM}}$ from the CM-system in the lab system[1] $\boldsymbol{E}$ and vice versa the following relationship is used:

$$E_{\text{CM}} = \frac{\boldsymbol{E}}{1 + \gamma_{\text{CM}}} \quad (2.5)$$

with $\gamma_{\text{CM}}$ as the Lorentz-factor for both protons in the CM-system, which is given by

$$\gamma_{\text{CM}} = \sqrt{\frac{\boldsymbol{E}}{2m_{\text{p}}c^2} + 1} \quad (2.6)$$

---

[1]if not stated otherwise, a bold $\boldsymbol{E}$ marks the kinetic energy of the incident proton in the lab system.

In case of unpolarized pp-scattering, the spin dependence term $\frac{(-1)^{2s}}{2s+1}$ of Eq. (2.3) results in $-\frac{1}{2}$.

Considering nuclear contributions one can efficiently analyse the scattering amplitudes by a partial wave expansion. With respect to this, one has to fullfil the Pauli's exclusion principle. The wave function of the two protons has to be antisymmetric under their exchange. Hence, a symmetric space wave function $(S, D, G, \ldots$-states) can only be associated with an antisymmetric spin wave function (even $J$, i. e. pp-singlet), whereas an antisymmetric space wave function $(P, F, \ldots$-states) requires a symmetric spin wave function (odd $J$, i. e. pp-triplet). At $10\,\text{MeV}$ the cross section is dominated more than $99\,\%$ by $S$-wave scattering (3; 4). The contribution of the $P$-states increases with energy but still is a minor fraction below $30\,\text{MeV}$. In all cases, the $P$-wave scattering cross section is zero at $\theta_{\text{lab}} = 45°$ in the lab frame, due to the interference in the identical particle system. In the interesting energy range, higher order states (like $D$-states) have an even lower scattering amplitude than the $P$-states.

In the present analysis, a partial wave expansion for the angular momentum is used that is restricted to the angular momentum $L = 0, 1, 2$, respectively, the $S$, $P$ and $D$-states (9; 10):

$$\left(\frac{d\sigma}{d\Omega}\right)_{\text{CM}} = \left(\frac{d\sigma}{d\Omega}\right)_{\text{Mott}} + \left(\frac{d\sigma}{d\Omega}\right)_{\text{V}} + \sum_{i=0}^{2} \left(\frac{d\sigma}{d\Omega}\right)_{L=i} \tag{2.7}$$

with $\left(\frac{d\sigma}{d\Omega}\right)_{\text{V}}$ being a correction of the Mott cross section for the vacuum polarization effects and $\sum_{i=0}^{2} \left(\frac{d\sigma}{d\Omega}\right)_{L=i}$ is the contribution of the different partial waves.

The nuclear interaction terms from phase shift analysis are written as

$$\left(\frac{d\sigma}{d\Omega}\right)^S_{L=0} = \frac{\eta^2}{4k^2}\left[-\frac{2X_0}{\eta}\sin(\delta_0)\cos(\delta_0) + \left(\frac{2Y_0}{\eta} + \frac{4}{\eta^2}\right)\sin^2(\delta_0)\right] \qquad (2.8)$$

$$\left(\frac{d\sigma}{d\Omega}\right)^P_{L=1} = \frac{\eta^2}{4k^2}\left[-\frac{2X_1P_1}{\eta}Z_2 + \left(\frac{2Y_1P_1}{\eta} + \frac{4}{\eta^2}\right)Z_1 + \frac{4P_2}{\eta^2}Z_3\right] \qquad (2.9)$$

$$\left(\frac{d\sigma}{d\Omega}\right)^D_{L=2} = \frac{\eta^2}{4k^2}\left[-\frac{10X_2P_2}{\eta}\sin(\delta_d)\cos(\delta_d)\right.$$
$$+ \left(\frac{10Y_2P_2}{\eta} + \frac{100P_2^2}{\eta^2}\right)\sin^2(\delta_d) \qquad (2.10)$$
$$\left. + \frac{40P_2}{\eta^2}\sin(\delta_0)\sin(\delta_d)\cos(\delta_d - \delta_0 + \zeta)\right]$$

These terms depend on the phase shifts $\delta_0$ for S-wave scattering, $\delta_P^{(0)}, \delta_P^{(1)}, \delta_P^{(2)}$ for the P-wave scattering and on an effective D-wave phase shift $\delta_d$. The representation of the P-wave scattering is transformed using coupling parameters $Z_1$, $Z_2$ and $Z_3$:

$$Z_1 = \sin^2\left(\delta_P^{(0)}\right) + 3\sin^2\left(\delta_P^{(1)}\right) + 5\sin^2\left(\delta_P^{(2)}\right) \qquad (2.11)$$

$$Z_2 = \sin\left(\delta_P^{(0)}\right)\cos\left(\delta_P^{(0)}\right) + 3\sin\left(\delta_P^{(1)}\right)\cos\left(\delta_P^{(1)}\right)$$
$$+ 5\sin\left(\delta_P^{(2)}\right)\cos\left(\delta_P^{(2)}\right) \qquad (2.12)$$

$$Z_3 = \frac{3}{2}\sin^2\left(\delta_P^{(1)}\right) + \frac{7}{2}\sin^2\left(\delta_P^{(2)}\right)$$
$$+ 4\sin\left(\delta_P^{(2)}\right)\sin\left(\delta_P^{(0)}\right)\cos\left(\delta_P^{(2)} - \delta_P^{(0)}\right) \qquad (2.13)$$
$$+ 9\sin\left(\delta_P^{(2)}\right)\sin\left(\delta_P^{(1)}\right)\cos\left(\delta_P^{(2)} - \delta_P^{(1)}\right)$$

and the other used notations are

$$
\begin{aligned}
X_0 &= \frac{\cos\left(\eta\ln(\sin^2\frac{\theta_{\mathrm{CM}}}{2})\right)}{\sin^2\frac{\theta_{\mathrm{CM}}}{2}} + \frac{\cos\left(\eta\ln(\cos^2\frac{\theta_{\mathrm{CM}}}{2})\right)}{\cos^2\frac{\theta_{\mathrm{CM}}}{2}} \\
Y_0 &= \frac{\sin\left(\eta\ln(\sin^2\frac{\theta_{\mathrm{CM}}}{2})\right)}{\sin^2\frac{\theta_{\mathrm{CM}}}{2}} + \frac{\sin\left(\eta\ln(\cos^2\frac{\theta_{\mathrm{CM}}}{2})\right)}{\cos^2\frac{\theta_{\mathrm{CM}}}{2}} \\
X_1 &= \frac{\cos\left(\eta\ln(\sin^2\frac{\theta_{\mathrm{CM}}}{2})+\xi\right)}{\sin^2\frac{\theta_{\mathrm{CM}}}{2}} - \frac{\cos\left(\eta\ln(\cos^2\frac{\theta_{\mathrm{CM}}}{2})+\xi\right)}{\cos^2\frac{\theta_{\mathrm{CM}}}{2}} \\
Y_1 &= \frac{\sin\left(\eta\ln(\sin^2\frac{\theta_{\mathrm{CM}}}{2})+\xi\right)}{\sin^2\frac{\theta_{\mathrm{CM}}}{2}} - \frac{\sin\left(\eta\ln(\cos^2\frac{\theta_{\mathrm{CM}}}{2})+\xi\right)}{\cos^2\frac{\theta_{\mathrm{CM}}}{2}} \\
X_2 &= \frac{\cos\left(\eta\ln(\sin^2\frac{\theta_{\mathrm{CM}}}{2})+\zeta\right)}{\sin^2\frac{\theta_{\mathrm{CM}}}{2}} + \frac{\cos\left(\eta\ln(\cos^2\frac{\theta_{\mathrm{CM}}}{2})+\zeta\right)}{\cos^2\frac{\theta_{\mathrm{CM}}}{2}} \\
Y_2 &= \frac{\sin\left(\eta\ln(\sin^2\frac{\theta_{\mathrm{CM}}}{2})+\zeta\right)}{\sin^2\frac{\theta_{\mathrm{CM}}}{2}} + \frac{\sin\left(\eta\ln(\cos^2\frac{\theta_{\mathrm{CM}}}{2})+\zeta\right)}{\cos^2\frac{\theta_{\mathrm{CM}}}{2}} \\
\xi &= 2\arctan(\eta) \\
\zeta &= 2\arctan(\eta) + 2\arctan(\tfrac{1}{2}\eta) \\
P_1 &= P_{L=1}(\cos(\theta_{\mathrm{CM}})) = \cos(\theta_{\mathrm{CM}}) \text{ 1st Legendre polynomial} \\
P_2 &= P_{L=2}(\cos(\theta_{\mathrm{CM}})) = -\frac{1}{2} + \frac{3}{2}\cos(\theta_{\mathrm{CM}})^2 \text{ 2nd Legendre polynomial}
\end{aligned}
\tag{2.14}
$$

# Chapter 3

# PARAMETERIZATION

## 3.1 EXPERIMENTAL DATA

There are several experimental data pools for differential pp-scattering cross section $(\mathrm{d}\sigma/\mathrm{d}\Omega)_{\mathrm{pp}}(\theta, E)$ like (11) and EXFOR/CSISRS (12; 13). Experimental data have been pooled to parameterize the data between $\boldsymbol{E} = 1.855\ldots50.1\,\mathrm{MeV}$ and scattering angles $\theta_{\mathrm{CM}} > 20°$ in (2). The experimental data of $(\mathrm{d}\sigma/\mathrm{d}\Omega)_{\mathrm{pp}}(\theta)$ with references are shown for the lab sytem in Fig. 3.1.

## 3.2 EXPONENTIAL APPROXIMATION

This section gives a short overview on the 3-parameter exponential approximation as discussed in (2), where a detailed documentation of this approximation is given. The approximation is given by:

$$\frac{\mathrm{d}\sigma}{\mathrm{d}\Omega}(\boldsymbol{E}, \theta_{\mathrm{CM}}) = \left(\frac{\mathrm{d}\sigma}{\mathrm{d}\Omega}\right)_{\mathrm{Mott}} + A(\boldsymbol{E})\cdot\left(1 - e^{C(\boldsymbol{E})(B(\boldsymbol{E})+\theta_{\mathrm{CM}})}\right) \qquad (3.1)$$

where $(\mathrm{d}\sigma/\mathrm{d}\Omega)_{\mathrm{Mott}}$ is taken from Eq. (2.3) and $A(\boldsymbol{E})$, $B(\boldsymbol{E})$ and $C(\boldsymbol{E})$ are the least square fit parameters[1]. The parameters are parameterized depending on

---

[1]The Eq. (3.2)-(3.3) in (2) contains some typos, which are corrected here.
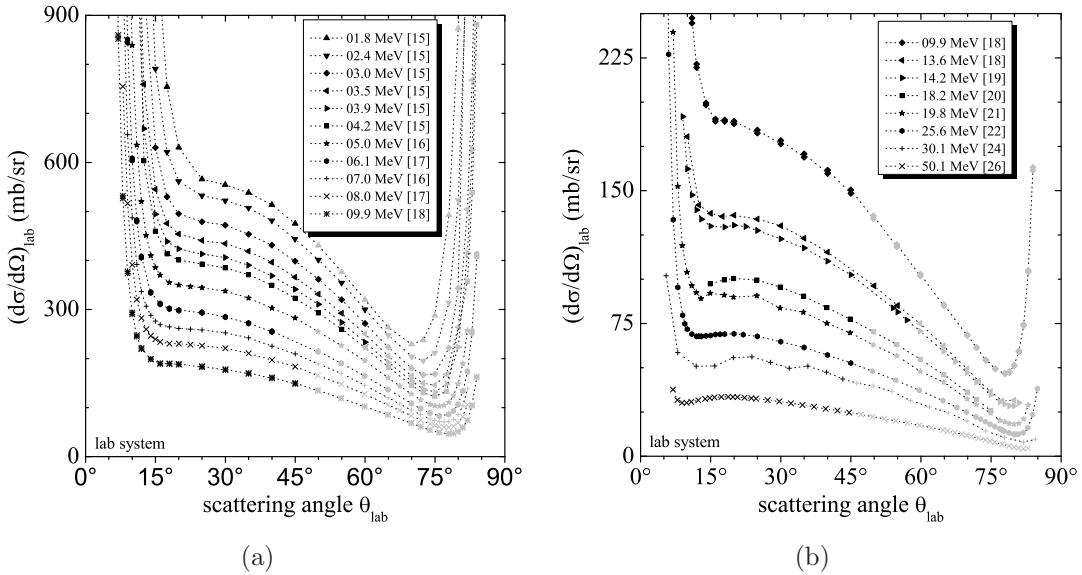
**Figure 3.1:** Elastic pp-scattering cross section data (lab system) (from (2)). Data points are connected for better visibility. Reported relative errors are smaller than $1\,\%$ for $\theta_{\text{lab}} = 20° \dots 70°$. This data and further data including inelastic scattering data are available in collection (11) or databases like EX-FOR/CSISRS (12; 13). Grey data points are calculated from symmetrical angles. Note that the differential cross section is symmetrical to $90°$ in the CM system, but not in the lab system due to $d\Omega$ transformation!

the kinetic energy in the lab system $\boldsymbol{E}$ with:

$$A(\boldsymbol{E}) \;=\; a_0 \left(1 + a_1 \boldsymbol{E}\right)^{-a_2} \tag{3.2}$$

$$B(\boldsymbol{E}) \;=\; b_0 + b_1 e^{b_2 \boldsymbol{E}} \tag{3.3}$$

$$C(\boldsymbol{E}) \;=\; c_0 + c_1 \boldsymbol{E} \tag{3.4}$$

The obtained values using in total 8 parameters $a_i$, $b_i$ and $c_i$ are listed in Table 3.1. Thus, we obtain pp-scattering cross sections in the CM-system as an analytical function of the CM-scattering angle $\theta_{\text{CM}} = 20° \dots 90°$ and kinetic energy $\boldsymbol{E} = 1.4\,\text{MeV} \dots 50.1\,\text{MeV}$ using Eq. (3.1) - (3.4). However, note that the accuracy of this fit is limited. For energies below $3\,\text{MeV}$, the fit does not represent the

data well. At higher energies, the deviations exceed $3\%$ only for few single data points, in particular at small scattering angles.

**Table 3.1:** Fit parameters for regression analysis of parameters $A(\boldsymbol{E})$, $B(\boldsymbol{E})$ and $C(\boldsymbol{E})$ with Eqs. (3.2)-(3.4). The Table is also an erratum of Table in (2).

| Parameter | Value | $\chi^2_{\text{red}}$ | $R^2_{\text{corr}}$ |
|---|---|---|---|
| $a_0$ ( mb/ sr) | $365 \pm 23$ | | |
| $a_1$ (1/ MeV) | $0.37 \pm 0.04$ | 32.6 | 0.9988 |
| $a_2$ | $1.267 \pm 0.024$ | | |
| $b_0$ (°) | $-14.92 \pm 0.14$ | | |
| $b_1$ (°) | $-36.6 \pm 1.9$ | 17.8 | 0.9838 |
| $b_2$ (1/ MeV) | $-0.368 \pm 0.020$ | | |
| $c_0$ (1/°) | $(-78.6 \pm 2.4) \cdot 10^{-3}$ | 8.4 | 0.888 |
| $c_1$ (1/° MeV) | $(-1.68 \pm 0.13) \cdot 10^{-3}$ | | |

# 3.3  EVALUATION OF THE EXPONENTIAL APPROXIMATION

For quantification of the goodness of the regression formula of Eq. (3.1) - (3.4) we have calculated the reduced least square function

$$\chi^2_{\mathrm{red}} = \frac{1}{N_{\mathrm{df}}} \sum_{j=1}^{n} \frac{\left( \frac{\mathrm{d}\sigma}{\mathrm{d}\Omega}_{\mathrm{pp}}(\boldsymbol{E_j}, \theta_j) - X(\boldsymbol{E_j}, \theta_j) \right)^2}{\Delta^2_{\mathrm{exp}}(\boldsymbol{E_j}, \theta_j)} \tag{3.5}$$

with the experimental data $X_j$ including its experimental errors $\Delta_{\mathrm{exp},j}$. The value $N_{\mathrm{df}}$ is the reduced number of degrees of freedome that is given by $N_{\mathrm{df}} = n - p$ with $n = 566$ data points and $p = 8$ parameters. As a second parameter for the goodness of the fit we calculated the correlation parameter:

$$R^2_{\mathrm{corr}} = 1 - \frac{\frac{1}{n-p-1} \sum_{j=1}^{n} \left( X(\boldsymbol{E_j}, \theta_j) - \frac{\mathrm{d}\sigma}{\mathrm{d}\Omega}_{\mathrm{pp}}(\boldsymbol{E_j}, \theta_j) \right)}{\frac{1}{n-1} \sum_{j=1}^{n} \left( X_j - \bar{X} \right)} \tag{3.6}$$

with $\bar{X}$ for an averaged value of the data. The goodness of fit coefficient $\chi^2_{\mathrm{red}}$ describes the mean square deviation relative to the experimental error $\Delta_{\mathrm{exp}}$. For $\chi^2_{\mathrm{red}} = 1$ the deviation of the fit function could be explained by the experimental errors, otherwise the value is $> 1$. The $R^2_{\mathrm{corr}}$ coefficient can get values between $0 \ldots 1$. For $R^2_{\mathrm{corr}} = 1$ the function is correlated with the dataset and for $R^2_{\mathrm{corr}} = 0$ uncorrelated. The calculated values of $\chi^2_{\mathrm{red}}$ and $R^2_{\mathrm{corr}}$ for the fitted parameters are listed in Table 3.1. The $R^2_{\mathrm{corr}} = 0.9988$ shows a good correlation of the fit with the data. The $\chi^2_{\mathrm{red}}$, however, has an value of 32.6 for the parameter $A(\boldsymbol{E})$ which indicates an inefficient fitting function. This could be problematical for interpolations and extrapolations.

For hydrogen analysis, angles $\theta_{\mathrm{CM}} > 50°$ are used in general. Here, the data are fitted with deviations better than $1\,\%$, which is in the range of the reported experimental errors and hence the fit is suitable for many quantification pur-

poses. Also, note that the fit function is only to be used for $\theta_{\text{CM}} \leq 90°$, but the scattering cross section is symmetrical to 90° in the CM-system anyway. The parameterization of Eq. (3.1) - (3.4) using the parameters from Table 3.1 are shown exemplarily for selected energies in Fig. 3.5 (tagged as EV2).

# 3.4 REGRESSION BY PHASE SHIFT ANAL- YSIS

In order to obtain a fit of $(\text{d}\sigma/\text{d}\Omega)_{\text{pp}}$ with a higher accuracy we utilize the phase shift analysis of Section 2 according to Eq. (2.7) - (2.14). In a first step, the phase shifts $\delta_0$, $\delta_d$ and the three coupling parameters $Z_1$, $Z_2$ and $Z_3$ are fitted for each energy where a complete data set of $(\text{d}\sigma/\text{d}\Omega)_{\text{pp}}(\theta)$ existed. The fitting of the three coupling parameters $Z_i$ was introduced instead of fitting $\delta_P^{(i)}$ because of a better convergence behavior. Initial values for the phase shifts $\delta_0$, $\delta_P^{(0)}$, $\delta_P^{(1)}$, $\delta_P^{(2)}$ were taken from (10) in the energy range of $1.855\ldots3.037\,\text{MeV}$ in order to obtain a stable fit behavior. For further regression computations at higher energies, the set of parameters at one energy was used as the initial values of the fit at the next higher energy. In (10) or other physical phase shift calculations the data are corrected by the vacuum polarization contribution $\left(\frac{d\sigma}{d\Omega}\right)_{\text{V}}$. In first calculations we saw, that a fit without considering explicitly the vacuum polarisation contribution has the same significance than including the vacuum polarisation contribution. However, parameter fluctuations are larger when the vacuum polarisation was included. Hence we performed the fit without the term $\left(\frac{d\sigma}{d\Omega}\right)_{\text{V}}$ accepting that the physical meaning of the phase shift values for nuclear physics theory gets lost. Fig. 3.2 - 3.3 shows the phase shifts for S, P and D-state scattering resulting from the least square fits depending on the incident proton energy $\boldsymbol{E}$ (□). For comparison the computations from (5) are plotted therein as well (small (▷)-data points with chain line). Due to successive restriction of the angular range to scattering
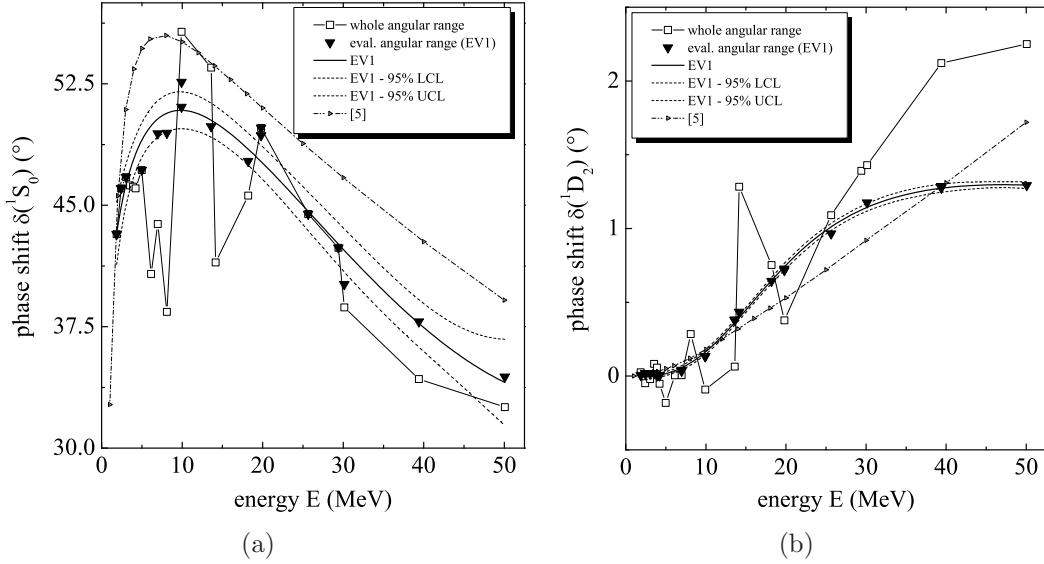
**Figure 3.2:** Calculated $^1S_0$ phase shift $\delta_0$ (a) and $^1D_2$ phase shift $\delta_d$ (b) in degrees vs particle energy $\boldsymbol{E}$. The data points ($\square$) (connected for better visibility) represent the calculations with full angular range compared to the ($\blacktriangledown$)-points in which the calculations are done by successive reduction of the angular range. For comparison, the connected smaller ($\triangleright$)-data points (chain line) are from other phase shift calculations (5). The solid line shows calculated parameterizations $\delta_{0,d}(\boldsymbol{E})$ of these phase shifts (EV1) as explained in Section 3.5 with 95% confidential intervals (dashed lines).

angles where mainly the nuclear part contributes to $(\mathrm{d}\sigma/\mathrm{d}\Omega)_{\mathrm{pp}}$ we obtain stable fits with a smooth energy dependence of the parameters ($\blacktriangledown$).
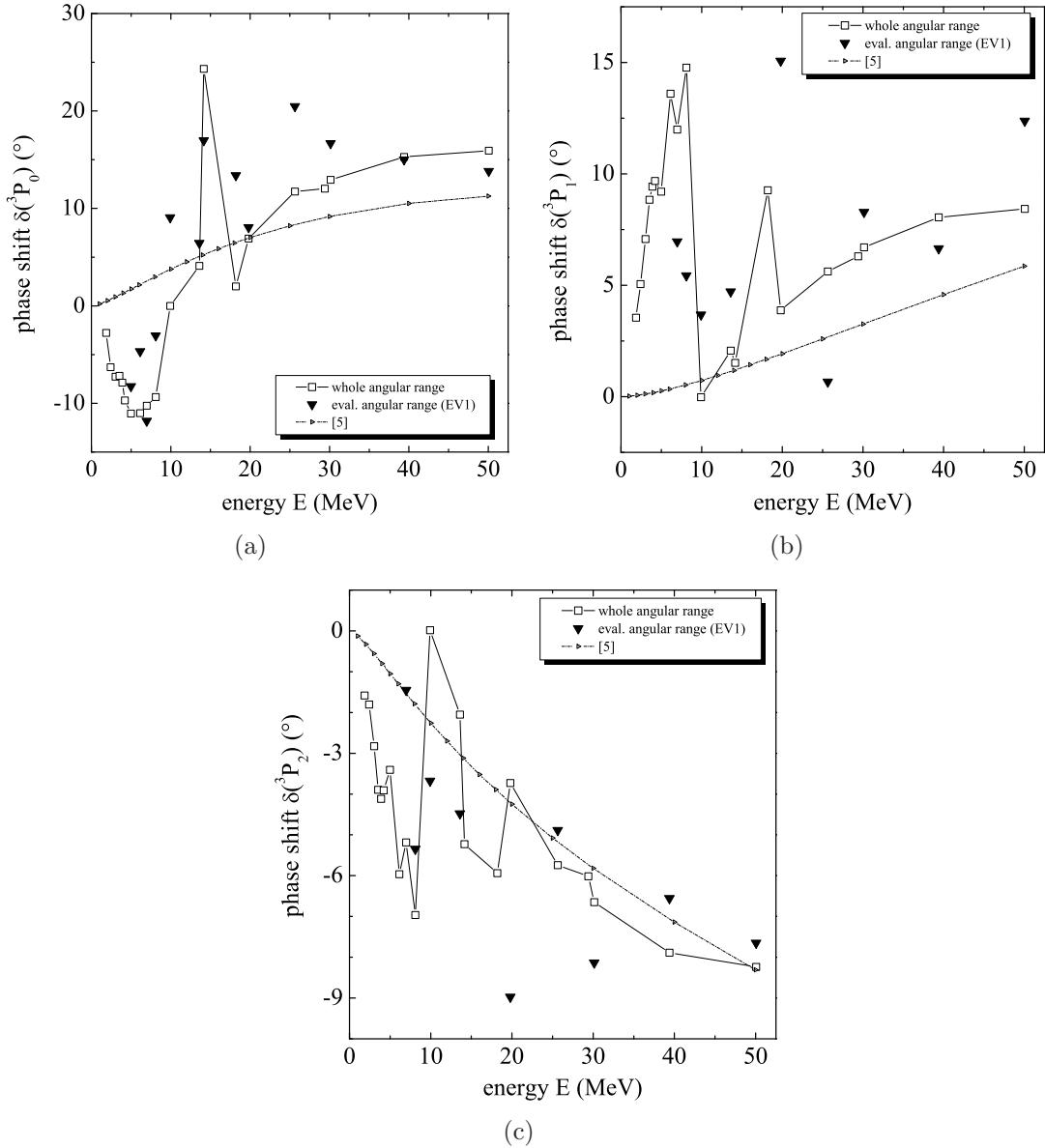
**Figure 3.3:** Calculated P-wave phase shifts $\delta_P^{(0)}$ (a), $\delta_P^{(1)}$ (b) and $\delta_P^{(2)}$ (c) in degrees vs particle energy $\boldsymbol{E}$. The data points ($\square$) (connected for better visibility) represent the calculations with full angular range compared to the ($\blacktriangledown$)-points in which the calculations are done by successive reduction of the angular range. For comparison, the connected smaller ($\triangleright$)-data points (chain line) are from other phase shift calculations (5).

(a)



(b)



(c)
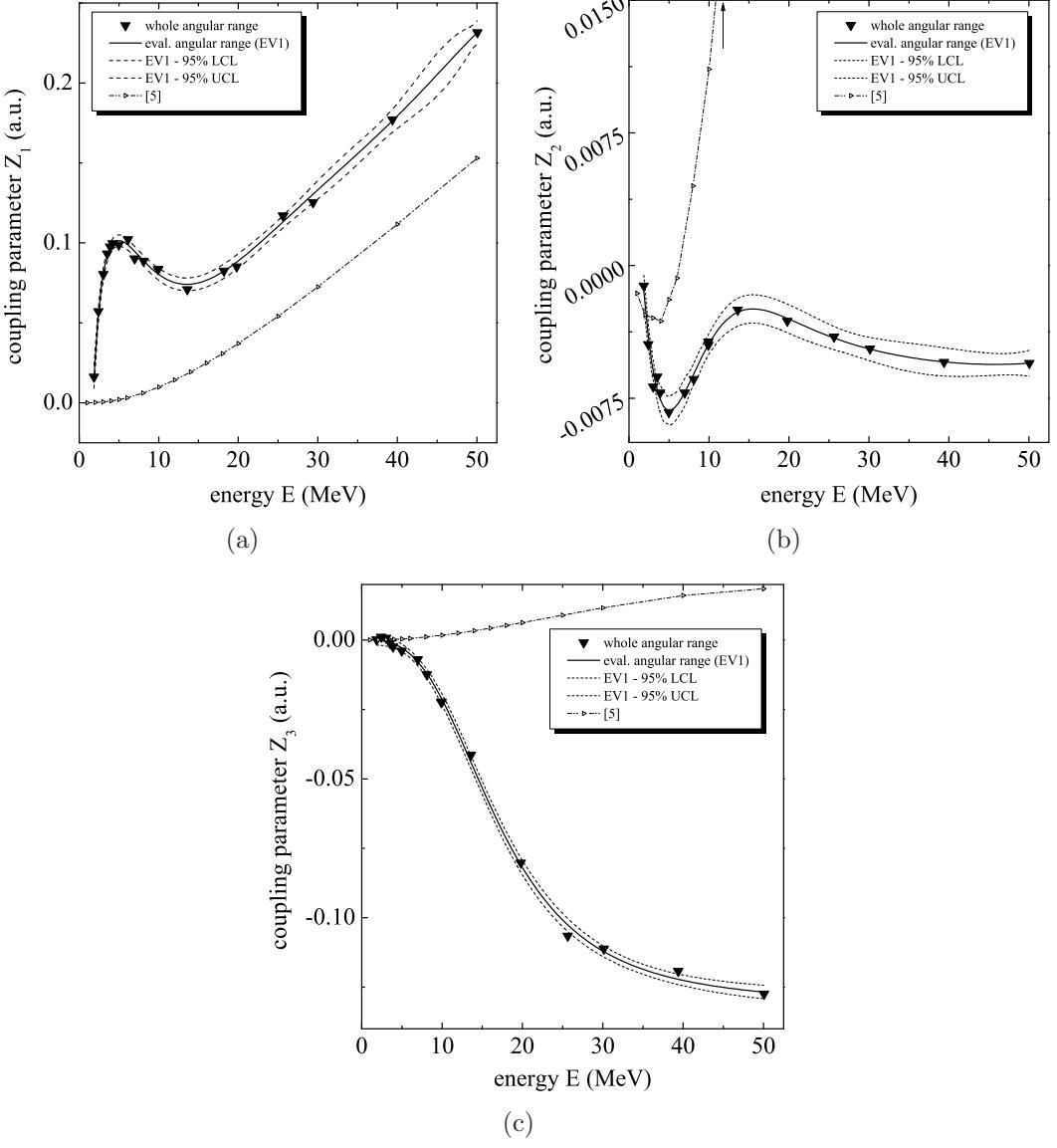
**Figure 3.4:** Calculated $Z_{1,2,3}$ coupling parameter for the P-wave phase shifts $\delta_P^{(i)}$ vs particle energy $\boldsymbol{E}$. The ($\blacktriangledown$)-points are calculated for the reduced angular range $\theta_{\mathrm{CM}} = 30° \ldots 150°$ of the angle range. For comparison, the connected smaller ($\triangleright$)-data points (chain line) are from other phase shift calculations (5). The solid line shows calculated parameterizations $Z_{1,2,3}(\boldsymbol{E})$ of these parameters as explained in Section 3.5 with 95% confidential intervals (dashed line).

# 3.5   PARAMETERIZATION OF THE PHASE SHIFT FUNCTION

In a second step, we fitted the energy dependent phase shifts as shown in Fig. 3.2 by the following functions.

$$\delta(^1S_0) = \delta_0(\boldsymbol{E}) = A_{\delta_0} + B_{\delta_0} \cdot \boldsymbol{E} + C_{\delta_0} \cdot \boldsymbol{E}^{\frac{1}{2}} + D_{\delta_0} \cdot \boldsymbol{E}^2 \tag{3.7}$$

$$\delta(^1D_2) = \delta_d(\boldsymbol{E}) = B_{\delta_d} + \frac{A_{\delta_d} - B_{\delta_d}}{1 + \left(\frac{\boldsymbol{E}}{C_{\delta_d}}\right)^{D_{\delta_d}}} + E_{\delta_d} \cdot \boldsymbol{E}^2 \tag{3.8}$$

In Fig. 3.2 we show the results of the calculated $\delta_0$ and $\delta_d$ phase shifts, with their computed regression parameters (Table 3.2).

First parameterization attempts of the P-state phase shifts $\delta_P^{(i)}$ (Fig. 3.3) showed a unstable behavior on the entire energy range. Oscillations occur due to a strong dependence of the parameterized $\delta_P^{(i)}$ phase shifts on each other. A direct fit of the coupling parameter $Z_i$ results in a much smoother behavior (Fig. 3.4) of the regression analysis for optimization of the fit functions of Eq. (3.9) - (3.11). In Fig. 3.4 the results of the calculated $Z_i$ parameter are presented, with their computed regression parameters (Table 3.2).

$$\begin{aligned} Z_1(\boldsymbol{E}) = {}& A_{Z_1} + B_{Z_1} \cdot \boldsymbol{E} + C_{Z_1} \cdot \boldsymbol{E}^2 + D_{Z_1} \cdot \boldsymbol{E}^3 \\ & + E_{Z_1} \cdot \boldsymbol{E}^4 + F_{Z_1} \cdot \boldsymbol{E}^5 + G_{Z_1} \cdot \boldsymbol{E}^{-1} + H_{Z_1} \cdot \boldsymbol{E}^{-2} \end{aligned} \tag{3.9}$$

$$\begin{aligned} Z_2(\boldsymbol{E}) = {}& A_{Z_2} + B_{Z_2} \cdot \boldsymbol{E} + C_{Z_2} \cdot \boldsymbol{E}^2 \\ & + (1 - D_{Z_2})e^{-E_{Z_2} \cdot \boldsymbol{E} + F_{Z_2}} \sin(G_{Z_2} \cdot \boldsymbol{E} + H_{Z_2}) \end{aligned} \tag{3.10}$$

$$Z_3(\boldsymbol{E}) = B_{Z_3} + \frac{A_{Z_3} - B_{Z_3}}{1 + \left(\frac{\boldsymbol{E}}{C_{Z_3}}\right)^{D_{Z_3}}} \tag{3.11}$$

**Table 3.2:** Calculated fit parameters for regression analysis of parameter $\delta_0$, $\delta_d$, $Z_1$,$Z_2$ and $Z_3$ with Eqs. (3.7) - (3.11).

| Function | Parameter | $i$ | Value | $\chi^2_{\mathrm{red}}$ | $R^2_{\mathrm{corr}}$ |
|---|---|---|---|---|---|
| $\delta_0(\boldsymbol{E})$ | $A_{\delta_0}$ $(°)$ | 1 | $25.5 \pm 3.0$ | 1.72 | 0.9306 |
| | $B_{\delta_0}$ $(°/\,\mathrm{MeV})$ | 2 | $-3.06 \pm 0.6$ | | |
| | $C_{\delta_0}$ $(°/\sqrt{\mathrm{MeV}})$ | 3 | $17.2 \pm 2.9$ | | |
| | $D_{\delta_0}$ $(°/\,\mathrm{MeV^2})$ | 4 | $(16 \pm 4.3) \cdot 10^{-3}$ | | |
| $\delta_d(\boldsymbol{E})$ | $A_{\delta_d}$ $(°)$ | 5 | $(-7.94 \pm 50) \cdot 10^{-3}$ | $5.28 \cdot 10^{-4}$ | 0.9979 |
| | $B_{\delta_d}$ $(°)$ | 6 | $1.58 \pm 0.15$ | | |
| | $C_{\delta_d}$ $(\,\mathrm{MeV})$ | 7 | $20.1 \pm 1.9$ | | |
| | $D_{\delta_d}$ | 8 | $2.94 \pm 0.50$ | | |
| | $E_{\delta_d}$ $(°/\,\mathrm{MeV^2})$ | 9 | $(-7.37 \pm 2.44) \cdot 10^{-5}$ | | |
| $Z_1(\boldsymbol{E})$ | $A_{Z_1}$ $(°)$ | 10 | $0.459 \pm 0.028$ | $1.11 \cdot 10^{-5}$ | 0.9942 |
| | $B_{Z_1}$ $(1/\,\mathrm{MeV})$ | 11 | $(-56.06 \pm 3.79) \cdot 10^{-3}$ | | |
| | $C_{Z_1}$ $(1/\,\mathrm{MeV^2})$ | 12 | $(3.5 \pm 0.4) \cdot 10^{-3}$ | | |
| | $D_{Z_1}$ $(1/\,\mathrm{MeV^3})$ | 13 | $(-10.225 \pm 1.731) \cdot 10^{-5}$ | | |
| | $E_{Z_1}$ $(1/\,\mathrm{MeV^4})$ | 14 | $(1.4792 \pm 0.3190) \cdot 10^{-6}$ | | |
| | $F_{Z_1}$ $(1/\,\mathrm{MeV^5})$ | 15 | $(-8.3876 \pm 2.2719) \cdot 10^{-9}$ | | |
| | $G_{Z_1}$ $(\,\mathrm{MeV})$ | 16 | $(-829.8 \pm 82.3) \cdot 10^{-3}$ | | |
| | $H_{Z_1}$ $(\,\mathrm{MeV^2})$ | 17 | $(334.9 \pm 59.5) \cdot 10^{-3}$ | | |
| $Z_2(\boldsymbol{E})$ | $A_{Z_2}$ $(°)$ | 18 | $(1.8 \pm 5.6) \cdot 10^{-3}$ | $2.1 \cdot 10^{-7}$ | 0.9386 |
| | $B_{Z_2}$ $(1/\,\mathrm{MeV})$ | 19 | $(-3.23 \pm 9.59) \cdot 10^{-4}$ | | |
| | $C_{Z_2}$ $(1/\,\mathrm{MeV^2})$ | 20 | $(3.54 \pm 18.59) \cdot 10^{-6}$ | | |
| | $D_{Z_2}$ | 21 | $99.091 \pm 0.371$ | | |
| | $E_{Z_2}$ $(1/\,\mathrm{MeV})$ | 22 | $(24.8 \pm 14.7) \cdot 10^{-2}$ | | |
| | $F_{Z_2}$ | 23 | $1.52 \pm 0.32$ | | |
| | $G_{Z_2}$ $(\,\mathrm{rad}/\,\mathrm{MeV})$ | 24 | $(21.5 \pm 4.2) \cdot 10^{-2}$ | | |
| | $H_{Z_2}$ $(\,\mathrm{rad})$ | 25 | $2.85 \pm 0.30$ | | |
| $Z_3(\boldsymbol{E})$ | $A_{Z_3}$ | 26 | $(1.18 \pm 44.62) \cdot 10^{-4}$ | $3.48 \cdot 10^{-6}$ | 0.9987 |
| | $B_{Z_3}$ | 27 | $(-13.1 \pm 0.3) \cdot 10^{-2}$ | | |
| | $C_{Z_3}$ $(\,\mathrm{MeV})$ | 28 | $16.95 \pm 1.02$ | | |
| | $D_{Z_3}$ | 29 | $3.08 \pm 0.41$ | | |

# 3.6 COMPARISON TO EXPERIMENTAL DATA

The result of this work is a closed analytical function for $(d\sigma/d\Omega)_{\text{pp}}(\boldsymbol{E}, \theta)$ when using Eq. (2.7) and its energy dependent parameterizations of Eqs. (3.7) - (3.11) with the parameters of Table 3.2:

$$
\begin{aligned}
\left(\frac{d\sigma}{d\Omega}\right)_{\text{CM}} = \left(\frac{d\sigma}{d\Omega}\right)_{\text{Mott}} (\boldsymbol{E}, \theta_{\text{CM}}) &+ \left(\frac{d\sigma}{d\Omega}\right)_{L=0}^{S} (\delta_0(\boldsymbol{E}), \theta_{\text{CM}}) \\
&+ \left(\frac{d\sigma}{d\Omega}\right)_{L=1}^{P} (Z_{1,2,3}(\boldsymbol{E}), \theta_{\text{CM}}) \qquad (3.12) \\
&+ \left(\frac{d\sigma}{d\Omega}\right)_{L=2}^{D} (\delta_d(\boldsymbol{E}), \theta_{\text{CM}})
\end{aligned}
$$

In the following, we tag this evaluation as EV1 and the exponential evaluation from (2) as EV2. For a quantification of the goodness of the fits we calculated the residua $\Delta_{\text{res}}$ between fit function and experimental data as shown in Fig. 3.5 exemplarily for selected data sets. As a main result, the residua $\Delta_{\text{res}}$ are not larger than the experimental errors $\Delta_{\text{exp}}$. For validation of the complete fit, we calculate the averaged residua and experimental errors $\bar{\Delta}_{\text{res,exp}} = \frac{1}{N} \sum_{i=1}^{N} \Delta_{\text{res,exp}}$ in the angular range $\theta_{\text{CM}} = 30° \dots 150°$ and energy range $\boldsymbol{E} = 1.855 \dots 50.1 \, \text{MeV}$ for each data set, respectively.

In Fig. 3.6 we show the averaged residua $\bar{\Delta}_{\text{res}}$ ($\blacktriangle$, $\square$), the averaged experimental errors $\bar{\Delta}_{\text{exp}}$ ($\bullet$-points) of the data depending on the energy.

As a result, the averaged residua of the fit $\bar{\Delta}_{\text{res}}$ are always in the range of the experimental error $\bar{\Delta}_{\text{exp}}$. We calculated a $(\chi^2_{\text{red}})^{\dagger}$ using Eq. (3.5) for the single data fits and the correlation parameter $R^2$ using Eq. (3.6). The number $p$ of independent fit parameters is small compared to the number of data and thus, $p = 0$ is used for simplification. These values are tabulated in Table 3.3. Only few data sets with large variation of the data points (19.8 MeV, 30.1 MeV) show low $R^2$ values.

For the entire fits over 566 data points (fd = full data set) in the energy
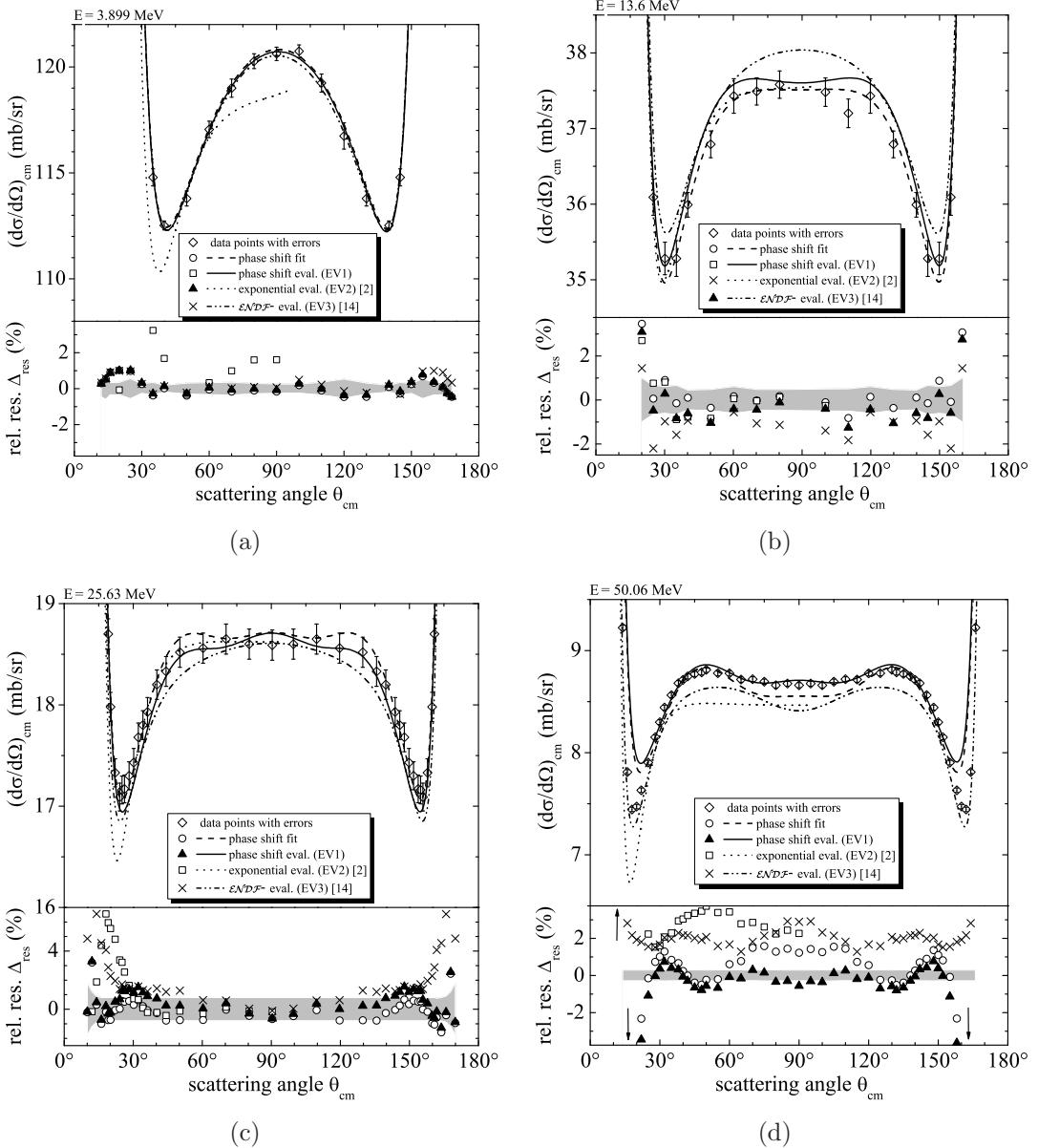
**Figure 3.5:** Elastic pp-scattering cross section data $(d\sigma/d\Omega)_{pp}$ ($\diamond$) for some selected energies with its experimental uncertainties (absolute: error bars; relative: gray band). Calculated regression curves from Eqs. (2.7) - (2.10) (dash line) and its relative residua $\Delta_{res}$ ($\circ$) are shown. In addition, the parameterized function (EV1) from Eqs. (3.7) - (3.11) (solid line) and its relative residua $\Delta_{res}$ ($\blacktriangle$) are plotted. For comparison, the simple exponential regression (EV2) from (2) (dotted line) from Eq. (3.1) and the $\mathcal{ENDF}$ evaluation (EV3) from (14) (chain line) and their relative residua $\Delta_{res}$ ($\square$, $\times$) are also plotted, respectively.
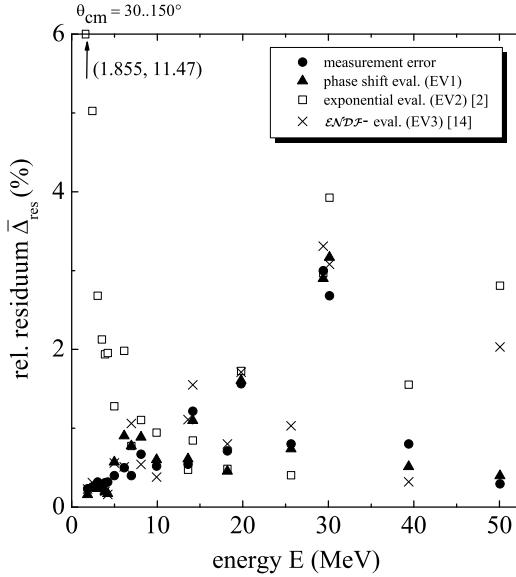
**Figure 3.6:** Calculated averaged relative residua $\bar{\Delta}_{\mathrm{res}}$ ($\blacktriangle$, $\square$, $\times$), averaged experimental relative error $\bar{\Delta}_{\mathrm{exp}}$ ($\bullet$) of the fit function $(\mathrm{d}\sigma/\mathrm{d}\Omega)_{\mathrm{pp}}(E,\theta)$ for the angle range $\theta_{\mathrm{CM}} = 30°\ldots150°$ and energy range $\boldsymbol{E} = 1.855\ldots50.1\,\mathrm{MeV}$, respectively.

range of $1.855\ldots50.1\,\mathrm{MeV}$ the fit procedure reached a $(\chi^2_{\mathrm{red}})_{\mathrm{fd}} = 7.03$. We see a discrepancy in the fit mainly at small angles where the Mott scattering cross section dominates and $(\mathrm{d}\sigma/\mathrm{d}\Omega)_{\mathrm{pp}}$ strongly varies with $\theta_{\mathrm{CM}}$. We speculate, whether the data may obtain larger errors or even systematic deviations in the measured scattering angles than cited, e.g. a misinterpreted mean scattering angle due to non-negligible detector aperture. However, we are only interested in $(\mathrm{d}\sigma/\mathrm{d}\Omega)_{\mathrm{pp}}$ for hydrogen analysis. Therefore we limited the angular range for fitting to $\theta_{\mathrm{CM}} \approx 30°\ldots150°$. Thus the number of data is reduced to 354 data points and we obtain $\chi^2_{\mathrm{red}} = 1.95$ and $R^2_{\mathrm{corr}} = 0.99992$. Also, the calculated $(\chi^2_{\mathrm{red}})^{\dagger}$ is mostly between $1\ldots3$ coupled with a $R^2$ value of mostly $0.8\ldots0.9$ that promised a good agreement to the experimental data. In Fig. 3.5 we show exemplarily for selected energies the results of the fitted functions compared to the parameterized function from Eq. 3.12 and the simple approximation from (2).

At energies below the last used data set of $\boldsymbol{E} = 1.855\,\mathrm{MeV}$, we exemplarily determined for the data set of $\boldsymbol{E} = 1.397\,\mathrm{MeV}$ an averaged residue of $\bar{\Delta}_{\mathrm{res}} \sim 3.5\%$

with a $\chi^2_{\mathrm{red}} = 105$. The latter number is $\gg 1$ which indicates an inadequate extrapolation of the existing parameterization, but this is mainly caused by the stated low experimental errors. As another reason we see in the single data set fit that the vacuum polarization contribution $\left(\frac{d\sigma}{d\Omega}\right)_{\mathrm{V}}$ becomes significant and cannot be compensated with our function where the physical effect of the vacuum polarization contribution is not included. Therefore, it would be the next step to implement such effects on this parameterization for calculations in the low energy range of $0.5\,\mathrm{MeV} \ldots 1.855\,\mathrm{MeV}$, as this has been done partly already in (10).

**Table 3.3:** Tabulated goodness parameters $\left(\chi^2_{\mathrm{red}}\right)^\dagger$ and $R^2$ see Eq. (3.6) and Eq. (3.5) of the single data fits with the fit restricted to a limited angular range. fd: full data set; NoP: number of points.

| Data set | energy $E$ [MeV] | $Range_{\mathrm{fd}}$ [°] | $NoP_{\mathrm{fd}}$ | $\left(\chi^2_{\mathrm{red}}\right)^\dagger_{\mathrm{fd}}$ | $Range_{\mathrm{fit}}$ [°] | $NoP_{\mathrm{fit}}$ | $\left(\chi^2_{\mathrm{red}}\right)^\dagger$ | $R^2$ |
|---|---|---|---|---|---|---|---|---|
| (15) | 1.855 | 14..166 | 23 | 2.51 | 30..150 | 15 | 0.75 | 0.9999 |
| (15) | 2.425 | 12..168 | 23 | 2.31 | 30..150 | 15 | 2.44 | 0.9992 |
| (15) | 3.037 | 12..168 | 25 | 2.19 | 30..150 | 15 | 1.12 | 0.9985 |
| (15) | 3.527 | 12..168 | 25 | 1.63 | 30..150 | 15 | 1.60 | 0.9962 |
| (15) | 3.899 | 12..168 | 25 | 1.33 | 30..150 | 15 | 0.66 | 0.9964 |
| (15) | 4.203 | 12..168 | 25 | 0.51 | 30..150 | 15 | 0.48 | 0.9957 |
| (16) | 4.978 | 16..164 | 33 | 2.84 | 30..150 | 19 | 2.57 | 0.9380 |
| (17) | 6.141 | 12..168 | 30 | 7.14 | 28..152 | 16 | 4.01 | 0.8450 |
| (16) | 6.968 | 16..164 | 33 | 5.25 | 28..152 | 21 | 5.23 | 0.8685 |
| (17) | 8.097 | 12..168 | 31 | 8.67 | 28..152 | 17 | 2.23 | 0.7242 |
| (18) | 9.918 | 20..160 | 19 | 7.10 | 30..150 | 15 | 2.34 | 0.8611 |
| (18) | 13.6 | 20.1..159.9 | 18 | 2.42 | 30..150 | 14 | 1.79 | 0.9249 |
| (19) | 14.16 | 18.1..161.9 | 29 | 1.39 | 30..150 | 19 | 1.36 | 0.7382 |
| (20) | 18.2 | 30..150 | 15 | 0.63 | 30..150 | 15 | 0.63 | 0.9499 |
| (21) | 19.8 | 14..166 | 29 | 1.94 | 30..150 | 15 | 2.34 | -0.0661 |
| (22) | 25.63 | 10.1..169.9 | 45 | 1.27 | 28..152 | 23 | 1.22 | 0.8875 |
| (23) | 29.4 | 24..156 | 18 | 2.07 | 32..148 | 16 | 1.39 | 0.5416 |
| (24) | 30.1 | 11..169 | 22 | 203.39 | 32..148 | 16 | 2.59 | 0.3332 |
| (25) | 39.4 | 8.1..171.9 | 53 | 42.17 | 27..153 | 25 | 0.61 | 0.9441 |
| (26) | 50.06 | 14..166 | 47 | 457.17 | 30..150 | 33 | 2.4 | 0.9080 |

# 3.7   COMPARISON TO $\mathcal{ENDF}$ CALCULATIONS

In order to get the most accurate parameterization for the differential cross section the validation with a closed theoretical calculation is indispensable. The data pool (27) provides the theoretical evaluation with the help of an R-matrix analysis with a maximum nuclear partial wave expansion of $L = 6$ of elastic pp scattering cross sections and polarization data with respect to an angular range $\theta_{\mathrm{CM}} = 0° \ldots 180°$ and energy range $\boldsymbol{E} = 0 \ldots 150\,\mathrm{MeV}$, respectively (14). The formula for calculating $(\mathrm{d}\sigma/\mathrm{d}\Omega)_{\mathrm{pp}}$ and its coefficients are described in the Evaluated Nuclear Data File ($\mathcal{ENDF}$) (27) and the 21 coefficients given for each energy are listed in the $\mathcal{ENDF}$-file (14). For this evaluation we use the abbreviation EV3, in contrast to EV1 and EV2.

For the evaluation of the goodness of EV3 we calculated the residua $\Delta_{\mathrm{res}}$ between EV3 and experimental data as shown in Fig. 3.5 exemplarily for selected data sets. In principal, the residua $\Delta_{\mathrm{res}}$ ($\times$ -points) are mostly out of the experimental uncertainties (gray-band) and larger than the EV1 residua, especially in the nuclear interaction range in which we are interested. We also calculated the averaged residua $\bar{\Delta}_{\mathrm{res}}$ ($\times$) and added this to Fig. 3.6 for each data set, respectively. Above $\sim 10\,\mathrm{MeV}$ $\bar{\Delta}_{\mathrm{res}}$ ($\times$) is always larger than the experimental uncertainties $\bar{\Delta}_{\mathrm{exp}}$ ($\bullet$) and the EV1 residua ($\blacktriangle$), except at $39.4\,\mathrm{MeV}$. For a more detailed analysis of the evaluation EV1 ($\blacktriangle$) and EV3 ($\times$) an angular and energy disperse evaluation of the goodness parameter $(\chi^2_{\mathrm{red}})^\dagger$ is shown in Fig. 3.7 and summarized in Table 3.4. Thus, we made two evaluations, one of the whole evaluated angular range $\theta_{\mathrm{CM}} = 30° \ldots 150°$ (see Fig. 3.7a) and one for the detector range $\theta_{\mathrm{lab}} = 25° \ldots 65°$ in which we are mainly interested with regard for hydrogen quantification. Due to symmetric behavior in the CM- system the calculation of the angular range $\theta_{\mathrm{CM}} = 50° \ldots 130°$ is useful (see Fig. 3.7b).

The differences of $(\chi^2_{\mathrm{red}})^\dagger$ between EV1 and EV3 below $\sim 10\,\mathrm{MeV}$ are small, but the $(\chi^2_{\mathrm{red}})^\dagger$ of EV3 is slightly better in this energy range. We also calculated a
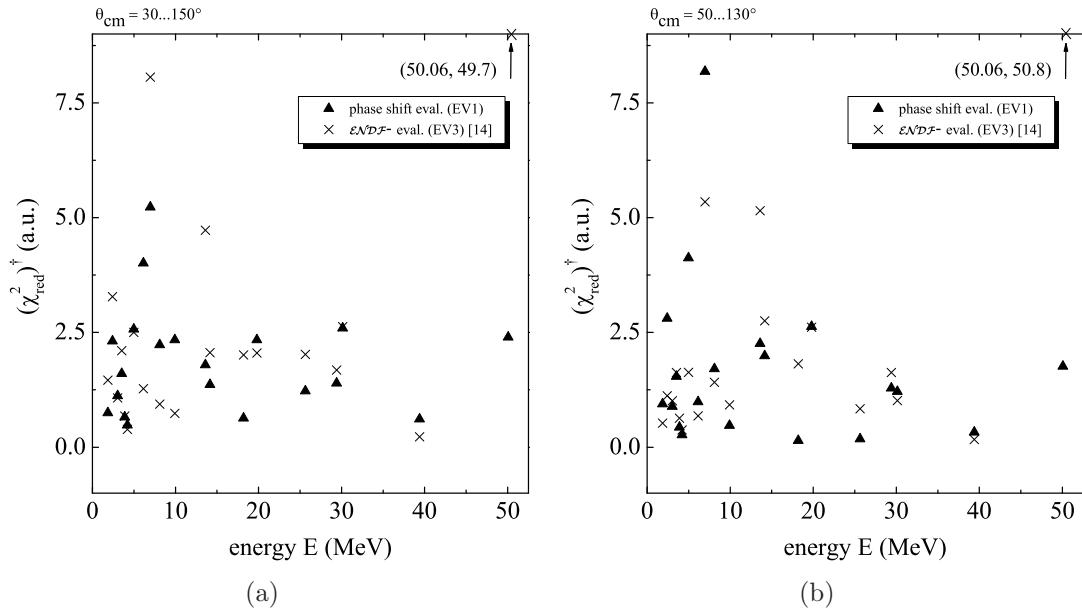
**Figure 3.7:** Calculated goodness parameters $\left(\chi^2_{\mathrm{red}}\right)^{\dagger}$ see Eq. (3.5) of the single data evaluations with the restriction to a limited angular range in a) for $\theta_{\mathrm{CM}} = 30°\ldots150°$ and b) for $\theta_{\mathrm{CM}} = 50°\ldots130°$. For comparison, both evaluations EV1 ($\blacktriangle$) and EV3 ($\times$) are plotted.

$\left(\chi^2_{\mathrm{red}}\right)^{\dagger}$ excluding the 6.968 MeV dataset, where $\left(\chi^2_{\mathrm{red}}\right)^{\dagger}$ shows a too large deviation to be included in an overall data evaluation. For the restricted angular range, at energies below $\sim 10\,\mathrm{MeV}$, the $\left(\chi^2_{\mathrm{red}}\right)^{\dagger}$ of EV3 is also slightly smaller (i.e. better) than $\left(\chi^2_{\mathrm{red}}\right)^{\dagger}$ of EV1. This is also conform with the whole data set calculation of $\left(\chi^2_{\mathrm{red}}\right)^{\dagger}$ in Table 3.4 for the energy range $1.9\ldots10.0\,\mathrm{MeV}$. However, for energies above $8.1\,\mathrm{MeV}$ the goodness parameter $\left(\chi^2_{\mathrm{red}}\right)^{\dagger}$ for EV3 is significantly larger, i.e. worse, than that of EV1, in particular for the $50.1\,\mathrm{MeV}$ dataset. The only exception is at $19.8\,\mathrm{MeV}$ and $39.4\,\mathrm{MeV}$, where $\left(\chi^2_{\mathrm{red}}\right)^{\dagger}$ of EV3 is slightly smaller than $\left(\chi^2_{\mathrm{red}}\right)^{\dagger}$ of EV1. This quantification is also conform with the full dataset evaluation in Table 3.4, in which the $\chi^2_{\mathrm{red}}$ parameter is calculated and listed for all energy ranges above $8.1\,\mathrm{MeV}$ and for the different angular restriction, respectively.

In summary, for the representation of the experimental data below $\sim 10\,\mathrm{MeV}$

**Table 3.4:** Tabulated goodness parameter $\left(\chi^2_{\mathrm{red}}\right)^{\dagger}$ for EV1 and EV3 evaluation of the whole dataset with the restriction to a limited angular and energy range. fd: full data set; NoP: number of points $n$; *without 6.968 MeV;

| $Range_{\mathrm{fit}}$ | $\theta_{\mathrm{CM}} = 30° \ldots 150°$ | | | $\theta_{\mathrm{CM}} = 50° \ldots 130°$ | | |
|---|---|---|---|---|---|---|
| | NoP | $EV1$ | $EV3$ | NoP | $EV1$ | $EV3$ |
| | $n$ | $p = 5$ | $p = 21$ | $n$ | $p = 0$ | $p = 0$ |
| $1.9 \ldots 10.0\,\mathrm{MeV}$ | 178 | 2.25 | 2.24 | 98 | 2.04 | **1.40** |
| $1.9 \ldots 10.0\,\mathrm{MeV}^*$ | 157 | 1.85 | **1.46** | 89 | 1.42 | **1.00** |
| $8.1 \ldots 50.1\,\mathrm{MeV}$ | 208 | **1.71** | 9.39 | 120 | **1.26** | 8.65 |
| $8.1 \ldots 39.4\,\mathrm{MeV}$ | 175 | **1.58** | 1.80 | 103 | **1.18** | 1.69 |
| | $n$ | $p = 29$ | $p = 21$ | $n$ | $p = 29$ | $p = 21$ |
| $1.9 \ldots 50.1\,\mathrm{MeV}$ | 354 | **1.95** | 6.98 | 200 | **1.94** | 6.45 |

both evaluations (EV1, EV3) have similar quality. However, EV1 represents the experimental data above 8.1 MeV better than EV3. We speculate, whether this significant discrepancy is caused by too few freedom parameters of EV3 at small angles where the Coulomb interaction dominates (Mott-scattering): There we find a steep gradient in the differential cross section $(\mathrm{d}\sigma/\mathrm{d}\Omega)_{\mathrm{pp}}(\theta)$. A small scattering angle mismatch $\triangle\theta$ due to misinterpretation of the mean detector angle could cause a "runaway" of the fit parameters and therefore a deviation at larger angles where nuclear scattering dominates. We saw a similar behavior of our fit (EV1) when we included the data at small scattering angles with the consequence that the representation is worse at the larger angles. Thus, a restriction of the angular fit range helps for the convergence of the fit at larger angles.

# 3.8   QUALITY OF THE PARAMETERIZED FUNCTION

The statistical error for each $(d\sigma/d\Omega)_{pp}$- value calculated from EV1 is evaluated at all angles between $\theta_{CM} = 30° \ldots 150°$ and energies in the range of $1.855 \ldots 50.1$. We define the least square function

$$\chi^2(A_i) = \sum_{j=1}^{n} \frac{\left( \frac{d\sigma}{d\Omega}_{pp}(A_i, \boldsymbol{E_j}, \theta_j) - X(\boldsymbol{E_j}, \theta_j) \right)^2}{\Delta_{\exp}^2(\boldsymbol{E_j}, \theta_j)} \tag{3.13}$$

with $A_i$ for the fit parameters[2], using the differential cross sections $(d\sigma/d\Omega)_{pp}(A_i, \boldsymbol{E_j}, \theta_j)$ that are evaluated for $n = 354$ experimental data points $(\boldsymbol{E_j}, \theta_j)$ and the corresponding experimental data $X(\boldsymbol{E_j}, \theta_j)$ together with the experimental uncertainties $\Delta_{\exp}(\boldsymbol{E_j}, \theta_j)$.

From $\chi^2$ one gets, the covariance matrix $\boldsymbol{C_{ov}}$ for the fitting parameters $A_i$ as

$$\boldsymbol{C_{ov}} = 2 \cdot \left[ \frac{\partial^2 \chi^2(A_i)}{\partial A_i \partial A_k} \Big|_{\tilde{A}_{i,k}} \right]^{-1} \tag{3.14}$$

with $\tilde{A}_{i,k}$ as the expectancy values of Table 3.2. Since the $A_i$ are not statistically independent non–diagonal elements of the $\boldsymbol{C_{ov}}$ occur. The statistical error is obtained with the gradient $\nabla_{A_i}$ of the function multiplied by the covariance matrix $\boldsymbol{C_{ov}}$. The relative experimental uncertainties $\Delta_{\exp}$ are low ($< 1\%$) compared to the number of free parameter (29) and there is a large number of data points (354). As a consequence, the statistical error $\Delta_{\text{stat}}(\boldsymbol{E}, \theta)$ of any differential cross section $(d\sigma/d\Omega)_{pp}$ is given by:

$$\Delta_{\text{stat}}(\boldsymbol{E}, \theta) = \left[ \nabla_{A_i} \left( \frac{d\sigma}{d\Omega}(\boldsymbol{E}, \theta, A_i) \right) \right]_{\tilde{A}_i}^{T} \cdot \boldsymbol{C_{ov}} \cdot \left[ \nabla_{A_i} \left( \frac{d\sigma}{d\Omega}(\boldsymbol{E}, \theta, A_i) \right) \right]_{\tilde{A}_i} \tag{3.15}$$

The covariance matrix $\boldsymbol{C_{ov}}$ has a cardinal number of $29 \times 29$ and is listed in

---

[2]The fit parameters $A_k$, $B_k$, $C_k$ from Table 3.2 are reduced to $A_i$ with $i = 1 \ldots 29$.

Table A.1. In Fig. 3.8a we show the computed results for $\Delta_{\mathrm{stat}}(\boldsymbol{E}, \theta)$ with Eq. (
3.15) as a normalized 2D-histogram.



(a)                                                          (b)
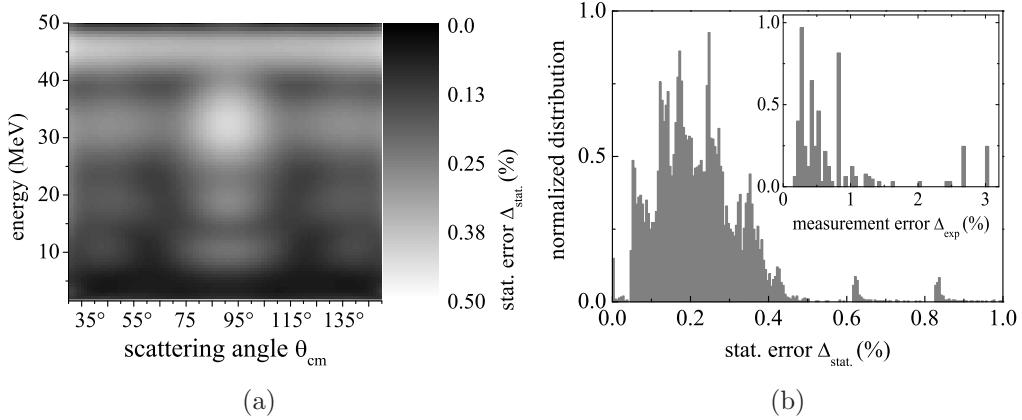
**Figure 3.8:** Calculated statistical error $\Delta_{\mathrm{stat}}$ for the $(\mathrm{d}\sigma/\mathrm{d}\Omega)_{\mathrm{pp}}(\boldsymbol{E}, \theta, A_i)$ function with the $\Delta_{\mathrm{stat}}(\boldsymbol{E}, \theta, A_i)$ function in a) a 2D–histogram and in b) as normalized distribution of the errors for the ranges $\theta_{\mathrm{CM}} = 30° \dots 150°$ and $E_{in} = 1.855 \dots 50.1\,\mathrm{MeV}$. For comparison, the normalized distribution of the experimental measurement error is also plotted.

Additionally, we plotted the distribution of the statistical error $\Delta_{\mathrm{stat}}$ in Fig. 3.8b. As a result, the average statistical error $\Delta_{\mathrm{stat}}$ is about 0.2% and most errors are less than 0.4%. This is smaller than the given average experimental uncertainty. The entire fit of $n = 354$ data points obviously enhances the statistical accuracy. Although, the cited experimental uncertainties $\Delta_{\mathrm{exp}}$ include systematical uncertainties $\Delta_{\mathrm{sys}}$ ($\Delta_{\mathrm{exp}} = \Delta_{\mathrm{stat,exp}} + \Delta_{\mathrm{sys}}$) the improvement is mainly regarded to the statistical uncertainties $\Delta_{\mathrm{stat}}$. As a consequence, quantification of hydrogen contents with an statistical accuracy in the 0.2% range is possible.

# 3.9   NUMERICAL APPROXIMATIONS

For a fast analysis the analytical function $(\mathrm{d}\sigma/\mathrm{d}\Omega)_{\mathrm{pp}}(\boldsymbol{E},\theta)$ is not practicable because of the long analytical expression. Hence, numerical tables that can be interpolated to any desired value are favorable for routine data analysis of hydrogen profiling. We give two $[\boldsymbol{E},\theta]$-matrices for numerical $(\mathrm{d}\sigma/\mathrm{d}\Omega)_{\mathrm{pp}}$ data: one for a quick evaluation in the lab system in Table 3.6). For the transformations from CM to lab system we used the equations as given in (2). The interpolation error $\Delta_{\mathrm{int}}$ of two points of this table is $< 0.8\%$. For computations a second table is calculated with an interpolation error of $\Delta_{\mathrm{int}} \approx \frac{1}{10}\Delta_{\mathrm{stat}}$. These data will be included on the website SigmaCalc (28) for nuclear cross sections. The tables for a fast analysis could also be found in the internet for free download (29) to be included into data evaluation software. The interpolation errors of both representations are plotted depending on the scattering angle in Fig. 3.9a and depending on the energy in Fig. 3.9b. The entire error for the analysis for the differential scattering cross section is given by

$$\Delta_{d\sigma/d\Omega} = \sqrt{(\Delta_{\mathrm{stat}})^2 + (\Delta_{\mathrm{int}})^2} \tag{3.16}$$

When using the accurate numerical table the error is dominated by the $\Delta_{\mathrm{stat}}$ and therefore $\Delta_{d\sigma/d\Omega} \approx \Delta_{\mathrm{stat}}$.
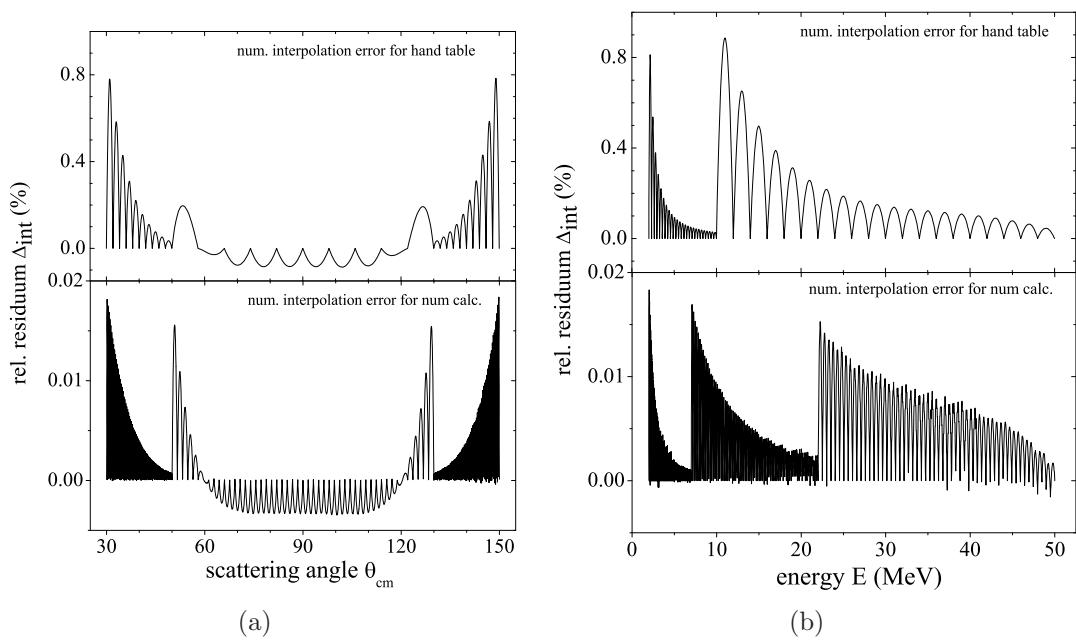
**Figure 3.9:** Calculated interpolation relative residua $\Delta_{\text{int}}$ (of two points) for the highest gradient of the angle (CM-system) (a) and for the energy (b).

**Table 3.5:** Computed differential cross section data matrix $d\sigma/d\Omega(\theta_{\mathrm{CM}}, \boldsymbol{E})$ in mb/sr for pp-scattering in the CM system for different angles and energies. The interpolation error $\Delta_{\mathrm{int}}$ of each point can be determined from Fig. 3.9. A matrix with a fine grid is available in (29).

| $E$ (MeV) | \(\theta_{\mathrm{CM}}\) (deg) 30 | 32 | 34 | 36 | 38 | 40 | 42 | 44 | 46 | 48 | 50 | 58 | 66 | 74 | 82 | 90 | 98 | 106 | 114 | 122 | 130 | 132 | 134 | 136 | 138 | 140 | 142 | 144 | 146 | 148 | 150 |
|---|---|---|---|---|---|---|---|---|---|---|---|---|---|---|---|---|---|---|---|---|---|---|---|---|---|---|---|---|---|---|---|
| 2 | 254.1 | 218.4 | 194.9 | 179.3 | 169.1 | 162.7 | 158.5 | 156.1 | 154.8 | 154.3 | 154.4 | 157.2 | 160.6 | 163.4 | 165.1 | 165.8 | 165.1 | 163.6 | 160.8 | 157.3 | 154.4 | 154.3 | 154.8 | 156.1 | 158.4 | 162.6 | 169.2 | 179.6 | 194.7 | 219.4 | 254.3 |
| 2.32 | 214.9 | 190.0 | 174.1 | 163.3 | 156.7 | 152.5 | 150.1 | 148.8 | 148.2 | 148.3 | 148.6 | 151.6 | 154.8 | 157.1 | 158.7 | 159.1 | 158.7 | 157.3 | 154.9 | 151.8 | 148.8 | 148.3 | 148.2 | 148.8 | 150.0 | 152.5 | 156.6 | 163.6 | 173.9 | 190.3 | 215.2 |
| 2.64 | 187.5 | 169.3 | 157.7 | 150.2 | 145.7 | 142.9 | 141.6 | 140.8 | 140.8 | 141.1 | 141.5 | 144.5 | 147.4 | 149.5 | 150.8 | 151.2 | 150.8 | 149.7 | 147.6 | 144.7 | 141.7 | 141.1 | 140.8 | 140.8 | 141.3 | 143.0 | 145.5 | 150.4 | 157.6 | 169.2 | 187.7 |
| 2.96 | 166.8 | 153.1 | 144.4 | 139.0 | 135.9 | 134.0 | 133.3 | 133.0 | 133.1 | 133.6 | 134.1 | 136.9 | 139.5 | 141.3 | 142.5 | 142.9 | 142.5 | 141.5 | 139.7 | 137.1 | 134.3 | 133.6 | 133.1 | 133.0 | 133.1 | 134.0 | 135.7 | 139.2 | 144.4 | 153.4 | 167.0 |
| 3.28 | 150.8 | 140.1 | 133.7 | 129.5 | 127.3 | 126.2 | 125.7 | 125.7 | 126.0 | 126.5 | 127.0 | 129.7 | 132.1 | 133.7 | 134.7 | 135.0 | 134.7 | 133.9 | 132.2 | 129.9 | 127.2 | 126.5 | 126.0 | 125.7 | 125.6 | 126.0 | 127.3 | 129.7 | 133.5 | 140.6 | 150.8 |
| 3.6 | 137.5 | 129.2 | 124.1 | 121.1 | 119.4 | 118.7 | 118.4 | 118.5 | 119.0 | 119.5 | 120.0 | 122.6 | 124.7 | 126.1 | 127.0 | 127.3 | 127.0 | 126.3 | 124.9 | 122.8 | 120.2 | 119.5 | 119.0 | 118.6 | 118.4 | 118.5 | 119.4 | 121.0 | 123.9 | 129.2 | 137.5 |
| 3.92 | 126.5 | 119.8 | 115.8 | 113.5 | 112.3 | 111.9 | 111.8 | 112.1 | 112.5 | 113.0 | 113.7 | 115.9 | 117.9 | 119.1 | 120.0 | 120.2 | 120.0 | 119.3 | 118.0 | 116.1 | 113.7 | 113.0 | 112.5 | 112.0 | 111.8 | 111.7 | 112.3 | 113.4 | 115.6 | 119.5 | 126.5 |
| 4.24 | 117.2 | 111.8 | 108.6 | 106.8 | 105.9 | 105.7 | 105.8 | 106.1 | 106.6 | 107.1 | 107.7 | 109.8 | 111.5 | 112.7 | 113.4 | 113.7 | 113.4 | 112.9 | 111.7 | 110 | 107.6 | 107.1 | 106.6 | 106.1 | 105.8 | 105.5 | 105.9 | 106.7 | 108.5 | 111.8 | 117.2 |
| 4.56 | 109.2 | 104.7 | 102.1 | 100.8 | 100.1 | 100.0 | 100.2 | 100.5 | 101.0 | 101.5 | 102.1 | 104.1 | 105.6 | 106.7 | 107.4 | 107.6 | 107.4 | 106.9 | 105.8 | 104.2 | 102.1 | 101.5 | 101.0 | 100.5 | 100.2 | 99.96 | 100.0 | 100.6 | 101.9 | 104.7 | 109.0 |
| 4.88 | 102.1 | 98.40 | 96.33 | 95.24 | 94.86 | 94.82 | 95.05 | 95.41 | 95.86 | 96.38 | 96.88 | 98.78 | 100.2 | 101.2 | 101.8 | 101.9 | 101.8 | 101.4 | 100.4 | 98.9 | 96.93 | 96.42 | 95.90 | 95.40 | 95.01 | 94.77 | 94.75 | 95.17 | 96.18 | 98.36 | 102.1 |
| 5.2 | 96.05 | 92.94 | 91.25 | 90.39 | 90.13 | 90.2 | 90.47 | 90.85 | 91.30 | 91.77 | 92.26 | 94.04 | 95.35 | 96.22 | 96.73 | 96.89 | 96.79 | 96.33 | 95.48 | 94.14 | 92.32 | 91.81 | 91.34 | 90.81 | 90.42 | 90.12 | 90.03 | 90.33 | 91.10 | 92.89 | 95.91 |
| 5.52 | 90.51 | 87.89 | 86.48 | 85.85 | 85.69 | 85.81 | 86.10 | 86.50 | 86.93 | 87.40 | 87.86 | 89.51 | 90.71 | 91.48 | 91.93 | 92.09 | 91.98 | 91.58 | 90.81 | 89.6 | 87.90 | 87.44 | 86.96 | 86.48 | 86.07 | 85.74 | 85.6 | 85.77 | 86.37 | 87.82 | 90.38 |
| 5.84 | 85.57 | 83.37 | 82.20 | 81.72 | 81.63 | 81.81 | 82.13 | 82.53 | 82.95 | 83.38 | 83.83 | 85.37 | 86.47 | 87.18 | 87.59 | 87.72 | 87.62 | 87.28 | 86.58 | 85.46 | 83.88 | 83.43 | 82.98 | 82.49 | 82.08 | 81.75 | 81.58 | 81.64 | 82.07 | 83.29 | 85.42 |
| 6.16 | 81.07 | 79.20 | 78.22 | 77.89 | 77.87 | 78.08 | 78.39 | 78.79 | 79.20 | 79.63 | 80.04 | 81.50 | 82.52 | 83.19 | 83.55 | 83.68 | 83.59 | 83.26 | 82.62 | 81.58 | 80.08 | 79.67 | 79.24 | 78.77 | 78.38 | 78.02 | 77.8 | 77.81 | 78.14 | 79.13 | 80.94 |
| 6.48 | 77.01 | 75.42 | 74.66 | 74.36 | 74.42 | 74.66 | 74.98 | 75.36 | 75.76 | 76.16 | 76.57 | 77.92 | 78.87 | 79.45 | 79.79 | 79.90 | 79.82 | 79.53 | 78.94 | 77.99 | 76.59 | 76.19 | 75.79 | 75.34 | 74.96 | 74.59 | 74.35 | 74.29 | 74.55 | 75.34 | 76.89 |
| 6.8 | 73.46 | 72.09 | 71.47 | 71.29 | 71.37 | 71.61 | 71.95 | 72.34 | 72.71 | 73.12 | 73.49 | 74.76 | 75.64 | 76.17 | 76.48 | 76.57 | 76.50 | 76.25 | 75.71 | 74.83 | 73.51 | 73.14 | 72.74 | 72.31 | 71.94 | 71.58 | 71.31 | 71.24 | 71.37 | 72.03 | 73.36 |
| 7.12 | 70.07 | 68.88 | 68.37 | 68.25 | 68.37 | 68.64 | 68.98 | 69.34 | 69.74 | 70.10 | 70.46 | 71.65 | 72.47 | 72.96 | 73.22 | 73.3 | 73.24 | 73.00 | 72.52 | 71.71 | 70.49 | 70.12 | 69.74 | 69.34 | 68.96 | 68.60 | 68.33 | 68.19 | 68.26 | 68.81 | 69.97 |
| 7.44 | 66.92 | 65.93 | 65.51 | 65.44 | 65.61 | 65.88 | 66.20 | 66.56 | 66.95 | 67.30 | 67.63 | 68.76 | 69.51 | 69.97 | 70.21 | 70.28 | 70.23 | 70.01 | 69.57 | 68.81 | 67.66 | 67.31 | 66.95 | 66.56 | 66.18 | 65.83 | 65.57 | 65.39 | 65.41 | 65.86 | 66.84 |
| 7.76 | 64.08 | 63.20 | 62.89 | 62.87 | 63.05 | 63.34 | 63.66 | 64.02 | 64.37 | 64.71 | 65.02 | 66.09 | 66.78 | 67.20 | 67.41 | 67.48 | 67.43 | 67.24 | 66.84 | 66.14 | 65.05 | 64.72 | 64.38 | 64.01 | 63.65 | 63.30 | 63.01 | 62.82 | 62.82 | 63.17 | 64.00 |
| 8.08 | 61.49 | 60.71 | 60.48 | 60.49 | 60.70 | 60.99 | 61.32 | 61.65 | 62.00 | 62.32 | 62.64 | 63.64 | 64.28 | 64.64 | 64.83 | 64.91 | 64.85 | 64.68 | 64.32 | 63.67 | 62.64 | 62.34 | 62.01 | 61.64 | 61.30 | 60.95 | 60.67 | 60.46 | 60.41 | 60.70 | 61.43 |
| 8.4 | 58.96 | 58.34 | 58.15 | 58.22 | 58.42 | 58.70 | 59.03 | 59.37 | 59.70 | 60.00 | 60.30 | 61.25 | 61.84 | 62.16 | 62.34 | 62.39 | 62.36 | 62.20 | 61.87 | 61.28 | 60.31 | 60.02 | 59.71 | 59.36 | 59.01 | 58.68 | 58.38 | 58.17 | 58.10 | 58.29 | 58.91 |
| 8.72 | 56.74 | 56.20 | 56.05 | 56.13 | 56.37 | 56.66 | 56.98 | 57.29 | 57.62 | 57.92 | 58.20 | 59.08 | 59.62 | 59.93 | 60.07 | 60.11 | 60.09 | 59.95 | 59.66 | 59.11 | 58.21 | 57.93 | 57.63 | 57.29 | 56.96 | 56.63 | 56.33 | 56.10 | 55.99 | 56.18 | 56.68 |
| 9.04 | 54.60 | 54.15 | 54.07 | 54.17 | 54.41 | 54.70 | 55.01 | 55.33 | 55.64 | 55.92 | 56.19 | 57.03 | 57.53 | 57.79 | 57.92 | 57.97 | 57.94 | 57.81 | 57.56 | 57.06 | 56.20 | 55.94 | 55.64 | 55.32 | 54.99 | 54.68 | 54.37 | 54.14 | 54.03 | 54.12 | 54.56 |
| 9.36 | 52.60 | 52.22 | 52.14 | 52.28 | 52.54 | 52.82 | 53.14 | 53.44 | 53.75 | 54.02 | 54.27 | 55.07 | 55.53 | 55.76 | 55.87 | 55.90 | 55.89 | 55.78 | 55.55 | 55.08 | 54.27 | 54.04 | 53.75 | 53.43 | 53.13 | 52.81 | 52.51 | 52.28 | 52.13 | 52.19 | 52.57 |
| 9.68 | 50.75 | 50.42 | 50.41 | 50.55 | 50.82 | 51.10 | 51.41 | 51.71 | 51.99 | 52.26 | 52.50 | 53.25 | 53.68 | 53.89 | 53.97 | 54.00 | 53.99 | 53.91 | 53.70 | 53.27 | 52.51 | 52.27 | 52.00 | 51.70 | 51.39 | 51.09 | 50.80 | 50.54 | 50.39 | 50.42 | 50.72 |
| 10 | 49.03 | 48.76 | 48.77 | 48.94 | 49.19 | 49.48 | 49.78 | 50.06 | 50.34 | 50.60 | 50.83 | 51.54 | 51.93 | 52.11 | 52.17 | 52.20 | 52.19 | 52.13 | 51.94 | 51.55 | 50.84 | 50.60 | 50.35 | 50.06 | 49.77 | 49.46 | 49.17 | 48.90 | 48.74 | 48.75 | 49.01 |

Table 3.5: Computed cross section data matrix $d\sigma/d\Omega(\theta_{CM}, \boldsymbol{E})$ for pp-scattering continued...

| E (MeV) | 30 | 32 | 34 | 36 | 38 | 40 | 42 | 44 | 46 | 48 | 50 | 58 | 66 | 74 | 82 | 90 | 98 | 106 | 114 | 122 | 130 | 132 | 134 | 136 | 138 | 140 | 142 | 144 | 146 | 148 | 150 |
|---|---|---|---|---|---|---|---|---|---|---|---|---|---|---|---|---|---|---|---|---|---|---|---|---|---|---|---|---|---|---|---|
| 12 | 40.31 | 40.28 | 40.41 | 40.63 | 40.90 | 41.18 | 41.44 | 41.68 | 41.91 | 42.12 | 42.30 | 42.78 | 42.99 | 43.05 | 43.07 | 43.05 | 43.07 | 43.07 | 43.01 | 42.79 | 42.29 | 42.12 | 41.92 | 41.68 | 41.44 | 41.16 | 40.91 | 40.63 | 40.42 | 40.26 | 40.32 |
| 14 | 34.04 | 34.13 | 34.33 | 34.57 | 34.82 | 35.07 | 35.30 | 35.51 | 35.70 | 35.87 | 36.00 | 36.35 | 36.44 | 36.43 | 36.40 | 36.38 | 36.40 | 36.43 | 36.44 | 36.35 | 36.00 | 35.87 | 35.71 | 35.51 | 35.31 | 35.06 | 34.80 | 34.57 | 34.33 | 34.13 | 34.04 |
| 16 | 29.39 | 29.54 | 29.76 | 30.00 | 30.24 | 30.47 | 30.67 | 30.86 | 31.03 | 31.15 | 31.26 | 31.51 | 31.54 | 31.51 | 31.46 | 31.44 | 31.46 | 31.51 | 31.54 | 31.5 | 31.26 | 31.15 | 31.03 | 30.86 | 30.67 | 30.46 | 30.24 | 30.00 | 29.76 | 29.54 | 29.40 |
| 18 | 25.82 | 26.00 | 26.21 | 26.45 | 26.66 | 26.87 | 27.06 | 27.22 | 27.36 | 27.47 | 27.56 | 27.74 | 27.75 | 27.71 | 27.68 | 27.67 | 27.68 | 27.71 | 27.74 | 27.74 | 27.56 | 27.47 | 27.36 | 27.22 | 27.06 | 26.87 | 26.67 | 26.43 | 26.22 | 26.00 | 25.82 |
| 20 | 22.92 | 23.10 | 23.32 | 23.54 | 23.73 | 23.92 | 24.08 | 24.22 | 24.35 | 24.44 | 24.52 | 24.67 | 24.67 | 24.64 | 24.64 | 24.65 | 24.64 | 24.64 | 24.67 | 24.67 | 24.52 | 24.44 | 24.35 | 24.22 | 24.09 | 23.92 | 23.73 | 23.52 | 23.32 | 23.10 | 22.90 |
| 22 | 20.55 | 20.74 | 20.94 | 21.15 | 21.33 | 21.49 | 21.65 | 21.77 | 21.87 | 21.96 | 22.02 | 22.13 | 22.14 | 22.14 | 22.18 | 22.18 | 22.18 | 22.14 | 22.14 | 22.13 | 22.02 | 21.96 | 21.87 | 21.77 | 21.65 | 21.49 | 21.33 | 21.13 | 20.94 | 20.74 | 20.53 |
| 24 | 18.60 | 18.78 | 18.97 | 19.17 | 19.33 | 19.48 | 19.62 | 19.73 | 19.83 | 19.89 | 19.95 | 20.04 | 20.05 | 20.07 | 20.13 | 20.17 | 20.13 | 20.07 | 20.05 | 20.04 | 19.95 | 19.89 | 19.83 | 19.73 | 19.63 | 19.49 | 19.33 | 19.15 | 18.99 | 18.78 | 18.60 |
| 26 | 16.89 | 17.08 | 17.27 | 17.44 | 17.59 | 17.73 | 17.84 | 17.94 | 18.03 | 18.09 | 18.14 | 18.22 | 18.23 | 18.28 | 18.35 | 18.38 | 18.34 | 18.28 | 18.23 | 18.22 | 18.14 | 18.09 | 18.03 | 17.94 | 17.85 | 17.73 | 17.59 | 17.42 | 17.25 | 17.07 | 16.89 |
| 28 | 15.53 | 15.70 | 15.88 | 16.05 | 16.18 | 16.31 | 16.41 | 16.50 | 16.58 | 16.63 | 16.67 | 16.74 | 16.75 | 16.80 | 16.89 | 16.94 | 16.89 | 16.8 | 16.75 | 16.74 | 16.67 | 16.63 | 16.58 | 16.51 | 16.41 | 16.31 | 16.18 | 16.03 | 15.86 | 15.69 | 15.53 |
| 30 | 14.29 | 14.46 | 14.62 | 14.78 | 14.91 | 15.02 | 15.12 | 15.20 | 15.26 | 15.31 | 15.35 | 15.41 | 15.42 | 15.47 | 15.57 | 15.62 | 15.57 | 15.47 | 15.42 | 15.41 | 15.35 | 15.31 | 15.26 | 15.20 | 15.12 | 15.02 | 14.91 | 14.76 | 14.60 | 14.46 | 14.29 |
| 32 | 13.24 | 13.39 | 13.54 | 13.69 | 13.80 | 13.91 | 14.00 | 14.08 | 14.13 | 14.17 | 14.22 | 14.25 | 14.26 | 14.31 | 14.40 | 14.45 | 14.40 | 14.31 | 14.26 | 14.25 | 14.22 | 14.18 | 14.13 | 14.08 | 14.00 | 13.91 | 13.81 | 13.67 | 13.52 | 13.38 | 13.24 |
| 34 | 12.33 | 12.46 | 12.62 | 12.74 | 12.86 | 12.96 | 13.04 | 13.11 | 13.17 | 13.20 | 13.24 | 13.26 | 13.25 | 13.30 | 13.40 | 13.45 | 13.40 | 13.30 | 13.25 | 13.25 | 13.23 | 13.20 | 13.17 | 13.11 | 13.04 | 12.96 | 12.86 | 12.74 | 12.60 | 12.46 | 12.33 |
| 36 | 11.53 | 11.66 | 11.81 | 11.93 | 12.04 | 12.13 | 12.20 | 12.27 | 12.32 | 12.36 | 12.38 | 12.40 | 12.38 | 12.43 | 12.52 | 12.56 | 12.52 | 12.43 | 12.38 | 12.39 | 12.38 | 12.36 | 12.33 | 12.27 | 12.20 | 12.13 | 12.04 | 11.93 | 11.79 | 11.67 | 11.53 |
| 38 | 10.83 | 10.97 | 11.11 | 11.22 | 11.32 | 11.41 | 11.48 | 11.54 | 11.59 | 11.62 | 11.64 | 11.63 | 11.62 | 11.65 | 11.73 | 11.78 | 11.73 | 11.65 | 11.62 | 11.63 | 11.64 | 11.62 | 11.59 | 11.54 | 11.48 | 11.41 | 11.33 | 11.22 | 11.09 | 10.97 | 10.83 |
| 40 | 10.23 | 10.37 | 10.49 | 10.59 | 10.70 | 10.77 | 10.85 | 10.9 | 10.94 | 10.97 | 10.99 | 10.98 | 10.94 | 10.97 | 11.04 | 11.07 | 11.04 | 10.97 | 10.94 | 10.98 | 10.99 | 10.97 | 10.94 | 10.90 | 10.85 | 10.78 | 10.70 | 10.59 | 10.47 | 10.36 | 10.22 |
| 42 | 9.740 | 9.867 | 9.983 | 10.08 | 10.18 | 10.26 | 10.33 | 10.37 | 10.42 | 10.45 | 10.45 | 10.44 | 10.39 | 10.40 | 10.46 | 10.48 | 10.46 | 10.40 | 10.39 | 10.43 | 10.45 | 10.44 | 10.41 | 10.37 | 10.33 | 10.25 | 10.18 | 10.08 | 9.980 | 9.861 | 9.736 |
| 44 | 9.305 | 9.426 | 9.539 | 9.641 | 9.730 | 9.806 | 9.868 | 9.915 | 9.950 | 9.972 | 9.983 | 9.954 | 9.894 | 9.892 | 9.936 | 9.961 | 9.938 | 9.895 | 9.897 | 9.956 | 9.983 | 9.973 | 9.951 | 9.914 | 9.867 | 9.804 | 9.729 | 9.638 | 9.537 | 9.423 | 9.301 |
| 46 | 8.904 | 9.022 | 9.132 | 9.228 | 9.314 | 9.386 | 9.445 | 9.490 | 9.522 | 9.542 | 9.551 | 9.512 | 9.443 | 9.429 | 9.463 | 9.486 | 9.466 | 9.432 | 9.446 | 9.515 | 9.550 | 9.543 | 9.523 | 9.489 | 9.444 | 9.386 | 9.313 | 9.228 | 9.129 | 9.017 | 8.904 |
| 48 | 8.676 | 8.790 | 8.895 | 8.989 | 9.073 | 9.142 | 9.198 | 9.240 | 9.270 | 9.287 | 9.295 | 9.249 | 9.170 | 9.142 | 9.164 | 9.183 | 9.166 | 9.145 | 9.171 | 9.25 | 9.295 | 9.288 | 9.271 | 9.240 | 9.197 | 9.141 | 9.071 | 8.987 | 8.894 | 8.786 | 8.672 |
| 50 | 8.273 | 8.385 | 8.488 | 8.579 | 8.659 | 8.726 | 8.780 | 8.819 | 8.847 | 8.862 | 8.868 | 8.813 | 8.725 | 8.687 | 8.698 | 8.714 | 8.701 | 8.688 | 8.728 | 8.814 | 8.868 | 8.864 | 8.847 | 8.818 | 8.778 | 8.725 | 8.657 | 8.577 | 8.487 | 8.381 | 8.272 |

**Table 3.6:** Computed differential cross section data matrix $d\sigma/d\Omega(\theta_{\mathrm{lab}}, \boldsymbol{E})$ in mb/sr for pp-scattering in the lab system for different angles and energies. The interpolation error $\Delta_{\mathrm{int}}$ of each point can be determined from Fig. 3.9. A matrix with a fine grid is available in (29). The energy of this table is calculated in both systems (lab+CM) using Eq. (2.5) - (2.6).

| $E$ | $E_{\mathrm{CM}}$ | $\theta_{\mathrm{lab}}$ (deg) | | | | | | | | | | | | | | | | | | | | | | | | | | | | | |
|---|---|---|---|---|---|---|---|---|---|---|---|---|---|---|---|---|---|---|---|---|---|---|---|---|---|---|---|---|---|---|---|
| (MeV) | (MeV) | 15 | 16 | 17 | 18 | 19 | 20 | 21 | 22 | 23 | 24 | 25 | 29 | 33 | 37 | 41 | 45 | 49 | 53 | 57 | 61 | 65 | 66 | 67 | 68 | 69 | 70 | 71 | 72 | 73 | 74 | 75 |
| 2 | 0.999 | 983.2 | 839.6 | 747.1 | 683.9 | 640.9 | 612.6 | 592.5 | 580 | 570.5 | 565.5 | 560.7 | 550.4 | 539.0 | 521.9 | 499.0 | 468.7 | 434.6 | 393.3 | 350.4 | 305.4 | 261.3 | 251.2 | 242.1 | 234.0 | 227.4 | 222.6 | 220.4 | 221.6 | 228.7 | 240.7 | 263.6 |
| 2.32 | 1.16 | 831.9 | 730.7 | 666.9 | 622.2 | 593.2 | 573.5 | 560.4 | 552.1 | 545.8 | 542.8 | 538.9 | 530.1 | 519.2 | 501.8 | 478.8 | 449.8 | 417.0 | 378.1 | 337.6 | 294.3 | 251.6 | 241.1 | 231.6 | 222.8 | 215.0 | 208.6 | 203.9 | 201.8 | 203.7 | 209.4 | 222.9 |
| 2.64 | 1.32 | 725.4 | 650.7 | 603.7 | 571.9 | 551.5 | 537.7 | 529.0 | 523.2 | 518.6 | 516.4 | 513.5 | 505.6 | 494.7 | 477.5 | 455.3 | 427.7 | 396.5 | 359.6 | 321.7 | 280.7 | 239.6 | 229.6 | 220.1 | 211.1 | 202.6 | 195.6 | 189.4 | 185.3 | 184.6 | 186.2 | 194.4 |
| 2.96 | 1.479 | 645.7 | 589.8 | 554.1 | 530.1 | 515.3 | 505.3 | 498.7 | 494.5 | 492.0 | 490.0 | 487.7 | 480.4 | 469.2 | 452.2 | 431.6 | 404.6 | 374.6 | 341.2 | 304.7 | 266.1 | 227.2 | 217.1 | 208.1 | 199.1 | 190.8 | 183.1 | 176.7 | 171.7 | 168.9 | 169.6 | 173.1 |
| 3.28 | 1.639 | 582.9 | 539.1 | 512.0 | 493.5 | 481.6 | 475.1 | 469.5 | 467.0 | 465.1 | 463.2 | 461.1 | 454.1 | 443.1 | 427.0 | 407.1 | 381.6 | 353.3 | 322.1 | 287.9 | 251.6 | 214.9 | 205.4 | 196.7 | 187.8 | 179.6 | 171.9 | 165.3 | 159.6 | 155.8 | 154.4 | 156.1 |
| 3.6 | 1.799 | 532.2 | 497.4 | 475.5 | 461.5 | 452.0 | 447.0 | 442.7 | 440.7 | 439.3 | 437.7 | 435.8 | 429.7 | 418.6 | 402.7 | 384.1 | 359.9 | 333.5 | 303.8 | 272.0 | 237.9 | 203.1 | 194.0 | 185.6 | 177.2 | 169.5 | 161.7 | 155.1 | 149.1 | 144.8 | 142.1 | 142.4 |
| 3.92 | 1.959 | 489.9 | 461.6 | 444.6 | 433.0 | 425.6 | 422.1 | 418.3 | 416.9 | 415.7 | 414.6 | 412.9 | 406.5 | 396.1 | 381.0 | 363.2 | 340.1 | 315.3 | 287.5 | 257.4 | 225.3 | 192.2 | 183.8 | 175.8 | 167.8 | 160.2 | 152.7 | 146.1 | 140.0 | 135.3 | 132.1 | 130.9 |
| 4.24 | 2.119 | 453.9 | 430.5 | 416.6 | 407.1 | 401.0 | 398.0 | 395.5 | 394.2 | 393.5 | 392.2 | 391.1 | 384.8 | 374.6 | 360.2 | 343.0 | 321.2 | 297.8 | 271.8 | 243.3 | 212.9 | 181.9 | 173.8 | 166.3 | 158.6 | 151.4 | 144.1 | 137.7 | 131.6 | 126.7 | 123.3 | 121.3 |
| 4.56 | 2.279 | 423.4 | 403.5 | 392.0 | 384.2 | 379.4 | 377.3 | 374.9 | 373.7 | 373.2 | 372.1 | 371.1 | 364.8 | 355.1 | 341.1 | 325.2 | 304.5 | 282.3 | 257.4 | 230.9 | 202.2 | 172.6 | 164.9 | 157.8 | 150.4 | 143.5 | 136.5 | 130.3 | 124.2 | 119.2 | 115.6 | 112.9 |
| 4.88 | 2.438 | 395.1 | 379.4 | 370.0 | 363.2 | 360.0 | 357.5 | 356.3 | 355.5 | 354.3 | 353.5 | 352.3 | 346.8 | 337.3 | 324.2 | 308.3 | 288.7 | 267.3 | 244.2 | 218.7 | 191.7 | 163.8 | 156.6 | 149.8 | 142.8 | 136.2 | 129.6 | 123.4 | 117.3 | 112.3 | 108.6 | 105.5 |
| 5.2 | 2.598 | 372.0 | 358.0 | 350.4 | 344.9 | 341.9 | 339.9 | 338.9 | 338.2 | 337.2 | 336.4 | 335.2 | 329.7 | 320.7 | 307.9 | 292.5 | 274.2 | 254.0 | 231.8 | 208.0 | 182.3 | 155.8 | 149.1 | 142.5 | 135.9 | 129.5 | 123.1 | 117.2 | 111.3 | 106.3 | 102.6 | 99.14 |
| 5.52 | 2.758 | 350.2 | 339.0 | 332.2 | 327.4 | 325.0 | 323.3 | 322.4 | 321.9 | 321.0 | 320.3 | 319.1 | 314.2 | 305.2 | 292.8 | 277.8 | 260.6 | 241.3 | 220.4 | 197.9 | 173.6 | 148.5 | 141.9 | 135.7 | 129.3 | 123.2 | 117.1 | 111.4 | 105.7 | 100.8 | 96.64 | 93.42 |
| 5.84 | 2.918 | 331.3 | 321.5 | 315.7 | 311.7 | 309.8 | 308.4 | 307.6 | 307.3 | 306.4 | 305.7 | 304.6 | 299.6 | 290.9 | 279.1 | 264.8 | 248.5 | 230.0 | 210.1 | 188.6 | 165.6 | 141.5 | 135.5 | 129.5 | 123.4 | 117.6 | 111.7 | 106.1 | 100.6 | 95.77 | 91.65 | 88.22 |
| 6.16 | 3.077 | 314.0 | 305.5 | 300.5 | 297.1 | 295.4 | 294.3 | 293.7 | 293.3 | 292.6 | 292.0 | 290.9 | 286.0 | 277.6 | 266.3 | 252.6 | 237.0 | 219.4 | 200.4 | 180.0 | 158.0 | 135.3 | 129.4 | 123.7 | 117.8 | 112.2 | 106.6 | 101.2 | 95.89 | 91.18 | 87.07 | 83.63 |
| 6.48 | 3.237 | 298.3 | 290.7 | 286.6 | 283.6 | 282.4 | 281.4 | 280.8 | 280.6 | 279.8 | 279.2 | 278.1 | 273.4 | 265.3 | 254.3 | 241.3 | 226.3 | 209.5 | 191.4 | 172.0 | 151.0 | 129.4 | 123.7 | 118.3 | 112.7 | 107.3 | 101.9 | 96.74 | 91.56 | 86.94 | 82.89 | 79.42 |
| 6.8 | 3.397 | 285.1 | 277.9 | 274.2 | 272.3 | 271.0 | 270.1 | 269.8 | 269.4 | 268.9 | 267.9 | 267.3 | 262.6 | 254.4 | 243.6 | 231.2 | 216.7 | 200.6 | 183.5 | 164.7 | 144.9 | 124.1 | 118.7 | 113.5 | 108.1 | 103.0 | 97.65 | 92.62 | 87.81 | 83.34 | 79.11 | 75.75 |
| 7.12 | 3.557 | 271.9 | 265.6 | 262.4 | 260.8 | 259.7 | 259.0 | 258.7 | 258.2 | 257.8 | 256.8 | 256.3 | 251.7 | 243.7 | 233.3 | 221.4 | 207.4 | 192.0 | 175.6 | 157.7 | 138.9 | 119.0 | 113.8 | 108.8 | 103.6 | 98.73 | 93.63 | 88.77 | 84.09 | 79.72 | 75.59 | 72.23 |
| 7.44 | 3.716 | 259.8 | 254.2 | 251.4 | 250.0 | 249.2 | 248.6 | 248.2 | 247.8 | 247.4 | 246.6 | 246.0 | 241.6 | 233.8 | 223.9 | 212.3 | 198.9 | 184.2 | 168.5 | 151.3 | 133.3 | 114.2 | 109.2 | 104.4 | 99.50 | 94.76 | 89.86 | 85.19 | 80.63 | 76.42 | 72.36 | 69.03 |
| 7.76 | 3.876 | 248.6 | 243.7 | 241.2 | 240.1 | 239.4 | 238.9 | 238.7 | 238.3 | 238.0 | 237.0 | 236.5 | 232.1 | 224.6 | 215.0 | 203.9 | 190.9 | 176.8 | 161.9 | 145.4 | 128.1 | 109.8 | 105.0 | 100.4 | 95.66 | 91.11 | 86.39 | 81.87 | 77.46 | 73.33 | 69.39 | 66.09 |
| 8.08 | 4.036 | 238.5 | 234.1 | 232.0 | 231.0 | 230.4 | 230.0 | 229.8 | 229.4 | 229.1 | 228.2 | 227.6 | 223.6 | 216.2 | 206.8 | 196.1 | 183.6 | 170.1 | 155.7 | 139.8 | 123.4 | 105.7 | 101.1 | 96.65 | 92.13 | 87.72 | 83.19 | 78.78 | 74.53 | 70.56 | 66.66 | 63.37 |
| 8.4 | 4.195 | 228.9 | 225.0 | 223.1 | 222.5 | 222.0 | 221.6 | 221.4 | 221.1 | 220.8 | 219.9 | 219.4 | 215.2 | 208.1 | 198.9 | 188.5 | 176.5 | 163.6 | 149.7 | 134.6 | 118.8 | 101.8 | 97.38 | 93.11 | 88.73 | 84.51 | 80.12 | 75.87 | 71.74 | 67.85 | 64.09 | 60.80 |
| 8.72 | 4.355 | 220.1 | 216.9 | 215.7 | 214.6 | 214.4 | 213.9 | 213.9 | 213.6 | 213.1 | 212.4 | 211.7 | 207.6 | 200.4 | 191.8 | 181.4 | 170.0 | 157.8 | 144.3 | 129.7 | 114.4 | 98.17 | 93.87 | 89.81 | 85.46 | 81.45 | 77.26 | 73.14 | 69.14 | 65.30 | 61.75 | 58.42 |
| 9.04 | 4.515 | 212.0 | 209.2 | 208.1 | 207.3 | 206.9 | 206.7 | 206.6 | 206.4 | 205.9 | 205.2 | 204.5 | 200.4 | 193.5 | 185.1 | 174.9 | 164.0 | 152.2 | 139.2 | 125.2 | 110.5 | 94.84 | 90.72 | 86.79 | 82.58 | 78.67 | 74.62 | 70.62 | 66.77 | 63.01 | 59.51 | 56.27 |
| 9.36 | 4.674 | 204.1 | 201.7 | 200.7 | 200.1 | 199.9 | 199.6 | 199.6 | 199.3 | 198.9 | 198.2 | 197.6 | 193.5 | 186.7 | 178.5 | 168.8 | 158.2 | 146.8 | 134.3 | 120.9 | 106.7 | 91.60 | 87.60 | 83.82 | 79.76 | 76.00 | 72.08 | 68.20 | 64.46 | 60.81 | 57.40 | 54.20 |
| 9.68 | 4.834 | 196.9 | 194.7 | 194.0 | 193.4 | 193.2 | 193.0 | 193.1 | 192.8 | 192.3 | 191.7 | 191.1 | 187.1 | 180.5 | 172.5 | 163.1 | 152.8 | 141.8 | 129.7 | 116.8 | 103.1 | 88.60 | 84.73 | 81.06 | 77.16 | 73.52 | 69.71 | 65.96 | 62.32 | 58.76 | 55.42 | 52.29 |
| 10 | 4.993 | 190.2 | 188.4 | 187.7 | 187.1 | 187.0 | 186.9 | 186.9 | 186.7 | 186.2 | 185.7 | 185.0 | 181.1 | 174.6 | 166.8 | 157.6 | 147.6 | 137.1 | 125.4 | 113.0 | 99.80 | 85.80 | 82.05 | 78.53 | 74.72 | 71.18 | 67.50 | 63.85 | 60.3 | 56.84 | 53.60 | 50.51 |

Table 3.6: Computed cross section data matrix $d\sigma/d\Omega(\theta_{\mathrm{lab}}, \boldsymbol{E})$ for pp-scattering continued...

| $E$ | $E_{\mathrm{CM}}$ | $\theta_{\mathrm{lab}}$ (deg) | | | | | | | | | | | | | | | | | | | | | | | | | | | | | |
|---|---|---|---|---|---|---|---|---|---|---|---|---|---|---|---|---|---|---|---|---|---|---|---|---|---|---|---|---|---|---|---|
| (MeV) | (MeV) | 15 | 16 | 17 | 18 | 19 | 20 | 21 | 22 | 23 | 24 | 25 | 29 | 33 | 37 | 41 | 45 | 49 | 53 | 57 | 61 | 65 | 66 | 67 | 68 | 69 | 70 | 71 | 72 | 73 | 74 | 75 |
| **12** | **5.99** | 156.7 | 155.6 | 155.3 | 155.4 | 155.5 | 155.6 | 155.6 | 155.2 | 155.0 | 154.5 | 153.9 | 150.0 | 144.6 | 137.7 | 130.1 | 121.7 | 113.0 | 103.4 | 93.52 | 82.70 | 71.20 | 68.20 | 65.19 | 62.13 | 59.08 | 55.99 | 52.97 | 49.96 | 46.97 | 44.16 | 41.52 |
| **14** | **6.987** | 132.3 | 132.0 | 132.2 | 132.5 | 132.5 | 132.7 | 132.6 | 132.4 | 132.1 | 131.7 | 131.3 | 127.8 | 122.7 | 116.5 | 110.0 | 103.0 | 95.55 | 87.52 | 79.35 | 70.25 | 60.62 | 58.05 | 55.56 | 52.93 | 50.34 | 47.72 | 45.11 | 42.5 | 39.92 | 37.41 | 35.07 |
| **16** | **7.983** | 114.7 | 114.7 | 115.0 | 115.1 | 115.5 | 115.6 | 115.5 | 115.4 | 115.3 | 114.9 | 114.2 | 111.1 | 106.4 | 101.1 | 95.44 | 89.13 | 82.56 | 75.79 | 68.58 | 60.90 | 52.62 | 50.47 | 48.31 | 46.00 | 43.77 | 41.42 | 39.15 | 36.83 | 34.57 | 32.42 | 30.28 |
| **18** | **8.979** | 100.8 | 101.0 | 101.4 | 101.7 | 101.8 | 102.0 | 102.0 | 101.9 | 101.5 | 101.4 | 100.8 | 97.74 | 93.63 | 88.79 | 83.71 | 78.33 | 72.60 | 66.63 | 60.28 | 53.58 | 46.35 | 44.42 | 42.52 | 40.50 | 38.56 | 36.50 | 34.50 | 32.43 | 30.37 | 28.50 | 26.54 |
| **20** | **9.973** | 89.41 | 89.81 | 90.24 | 90.44 | 90.64 | 90.91 | 90.82 | 90.72 | 90.45 | 90.13 | 89.62 | 86.76 | 83.20 | 78.92 | 74.58 | 69.75 | 64.56 | 59.18 | 53.54 | 47.53 | 41.16 | 39.45 | 37.79 | 35.99 | 34.25 | 32.44 | 30.64 | 28.79 | 26.96 | 25.18 | 23.51 |
| **22** | **10.97** | 80.40 | 80.79 | 81.23 | 81.50 | 81.72 | 81.8 | 81.79 | 81.76 | 81.48 | 81.09 | 80.62 | 78.13 | 74.92 | 71.20 | 67.12 | 62.90 | 58.18 | 53.32 | 48.17 | 42.74 | 37.02 | 35.50 | 34.00 | 32.40 | 30.83 | 29.18 | 27.57 | 25.91 | 24.26 | 22.69 | 21.06 |
| **24** | **11.96** | 72.95 | 73.36 | 73.73 | 74.05 | 74.22 | 74.25 | 74.25 | 74.12 | 73.90 | 73.59 | 73.19 | 70.80 | 68.00 | 64.48 | 61.11 | 57.22 | 52.89 | 48.38 | 43.56 | 38.74 | 33.54 | 32.17 | 30.77 | 29.36 | 27.94 | 26.45 | 24.99 | 23.50 | 21.98 | 20.56 | 19.10 |
| **26** | **12.96** | 66.11 | 66.47 | 66.93 | 67.17 | 67.31 | 67.31 | 67.39 | 67.35 | 67.09 | 66.74 | 66.36 | 64.28 | 61.50 | 58.60 | 55.57 | 51.96 | 48.04 | 43.78 | 39.46 | 35.04 | 30.38 | 29.15 | 27.89 | 26.59 | 25.28 | 23.94 | 22.63 | 21.30 | 19.92 | 18.58 | 17.24 |
| **28** | **13.95** | 60.95 | 61.35 | 61.68 | 61.89 | 62.05 | 62.13 | 62.06 | 62.06 | 61.86 | 61.50 | 61.07 | 59.09 | 56.70 | 53.98 | 51.18 | 47.92 | 44.27 | 40.30 | 36.37 | 32.25 | 27.96 | 26.80 | 25.65 | 24.43 | 23.29 | 22.07 | 20.84 | 19.58 | 18.29 | 17.13 | 15.90 |
| **30** | **14.94** | 56.05 | 56.47 | 56.73 | 56.98 | 57.10 | 57.22 | 57.07 | 57.02 | 56.9 | 56.59 | 56.26 | 54.29 | 52.06 | 49.66 | 47.11 | 44.17 | 40.77 | 37.03 | 33.39 | 29.62 | 25.66 | 24.62 | 23.58 | 22.48 | 21.41 | 20.27 | 19.16 | 18.00 | 16.81 | 15.71 | 14.56 |
| **32** | **15.93** | 51.97 | 52.28 | 52.63 | 52.82 | 52.97 | 52.99 | 52.97 | 52.84 | 52.65 | 52.45 | 52.17 | 50.32 | 48.14 | 45.94 | 43.57 | 40.82 | 37.70 | 34.28 | 30.80 | 27.41 | 23.77 | 22.80 | 21.83 | 20.81 | 19.82 | 18.75 | 17.73 | 16.63 | 15.59 | 14.53 | 13.46 |
| **34** | **16.92** | 48.44 | 48.68 | 49.01 | 49.26 | 49.32 | 49.42 | 49.31 | 49.22 | 49.09 | 48.86 | 48.52 | 46.85 | 44.74 | 42.70 | 40.55 | 37.99 | 35.10 | 31.79 | 28.60 | 25.45 | 22.09 | 21.19 | 20.31 | 19.37 | 18.42 | 17.45 | 16.48 | 15.44 | 14.48 | 13.50 | 12.51 |
| **36** | **17.91** | 45.36 | 45.63 | 45.87 | 46.04 | 46.24 | 46.27 | 46.21 | 46.15 | 46.00 | 45.72 | 45.37 | 43.77 | 41.85 | 39.87 | 37.85 | 35.42 | 32.69 | 29.69 | 26.75 | 23.78 | 20.66 | 19.81 | 19.01 | 18.10 | 17.23 | 16.32 | 15.40 | 14.46 | 13.51 | 12.63 | 11.69 |
| **38** | **18.9** | 42.63 | 42.99 | 43.18 | 43.36 | 43.46 | 43.56 | 43.50 | 43.43 | 43.19 | 42.97 | 42.68 | 41.04 | 39.18 | 37.37 | 35.47 | 33.24 | 30.66 | 27.79 | 25.04 | 22.30 | 19.39 | 18.61 | 17.82 | 16.99 | 16.19 | 15.33 | 14.47 | 13.58 | 12.70 | 11.85 | 10.97 |
| **40** | **19.89** | 40.41 | 40.76 | 40.98 | 41.14 | 41.34 | 41.27 | 41.29 | 41.20 | 40.98 | 40.77 | 40.51 | 38.87 | 37.10 | 35.37 | 33.53 | 31.35 | 28.92 | 26.28 | 23.65 | 21.13 | 18.39 | 17.63 | 16.89 | 16.12 | 15.35 | 14.51 | 13.70 | 12.85 | 12.05 | 11.23 | 10.43 |
| **42** | **20.88** | 38.51 | 38.78 | 39.04 | 39.23 | 39.32 | 39.31 | 39.27 | 39.26 | 39.06 | 38.83 | 38.51 | 36.98 | 35.23 | 33.49 | 31.73 | 29.71 | 27.41 | 24.95 | 22.48 | 20.05 | 17.45 | 16.77 | 16.06 | 15.31 | 14.57 | 13.80 | 13.06 | 12.25 | 11.45 | 10.70 | 9.891 |
| **44** | **21.87** | 36.76 | 37.07 | 37.32 | 37.47 | 37.53 | 37.59 | 37.56 | 37.45 | 37.32 | 37.02 | 36.76 | 35.27 | 33.54 | 31.84 | 30.19 | 28.21 | 26.01 | 23.71 | 21.39 | 19.09 | 16.64 | 15.98 | 15.32 | 14.62 | 13.91 | 13.17 | 12.44 | 11.68 | 10.92 | 10.15 | 9.440 |
| **46** | **22.86** | 35.29 | 35.55 | 35.73 | 35.91 | 36.01 | 36.01 | 36.02 | 35.92 | 35.75 | 35.49 | 35.15 | 33.75 | 32.02 | 30.32 | 28.70 | 26.87 | 24.76 | 22.61 | 20.43 | 18.23 | 15.91 | 15.27 | 14.63 | 13.96 | 13.28 | 12.59 | 11.88 | 11.18 | 10.44 | 9.742 | 9.014 |
| **48** | **23.85** | 34.39 | 34.65 | 34.87 | 35.02 | 35.09 | 35.11 | 35.02 | 34.96 | 34.77 | 34.56 | 34.24 | 32.78 | 31.08 | 29.40 | 27.80 | 25.98 | 23.97 | 21.86 | 19.82 | 17.72 | 15.46 | 14.85 | 14.23 | 13.57 | 12.92 | 12.24 | 11.56 | 10.86 | 10.17 | 9.455 | 8.757 |
| **50** | **24.84** | 32.88 | 33.16 | 33.36 | 33.50 | 33.58 | 33.61 | 33.54 | 33.45 | 33.26 | 33.04 | 32.77 | 31.29 | 29.67 | 28.03 | 26.44 | 24.69 | 22.81 | 20.80 | 18.86 | 16.91 | 14.77 | 14.18 | 13.58 | 12.97 | 12.36 | 11.69 | 11.06 | 10.37 | 9.695 | 9.038 | 8.365 |

# Chapter 4

# CONCLUSION

Proton-proton scattering at MeV energies has proven to be the most sensitive method for hydrogen depth profiling at micrometer depth resolution without any need for reference standards when the differential scattering cross section $(\mathrm{d}\sigma/\mathrm{d}\Omega)_{\mathrm{pp}}$ is known.

We performed a phase shift analysis of experimental scattering cross section datasets, i.e. by fitting 354 data points in the energy range $1.9\dots50\,\mathrm{MeV}$ and laboratory scattering angles $\theta_{\mathrm{lab}} = 15°\dots75°$, resulting in total uncertainties that are below the measurement error. Thus, the differential cross section can be calculated for any energy and angle in the given intervals. For the parameterizations we determined an average statistical error $\Delta_{\mathrm{stat}}(\boldsymbol{E},\theta)$ of the $(\mathrm{d}\sigma/\mathrm{d}\Omega)_{\mathrm{pp}}(\boldsymbol{E},\theta)$ function as low as $\bar{\Delta}_{\mathrm{stat}}$ of 0.2% and a maximum error of $\sim 0.4\%$. A comparison with existing $\mathcal{ENDF}$-files (27) shows a better representation of the experimental data by our analysis ($\chi^2_{\mathrm{red}} = 1.95(\mathrm{EV1})$), especially for $\boldsymbol{E} > 8\,\mathrm{MeV}$, in contrast to the $\mathcal{ENDF}$-data ($\chi^2_{\mathrm{red}} = 6.98(\mathrm{EV3})$). For fast numerical calculations we computed two types of $[\boldsymbol{E},\theta]$-matrices, one for quick by hand evaluations with an interpolation error $\Delta_{\mathrm{int}}$ of $< 0.8\%$, and one for accurate computations with $\Delta_{\mathrm{int}} < 0.02\%$.

# Appendix A

# APPENDIX

**Table A.1:** Computed covariance matrix $(\mathcal{C}_{\mathbf{ov}})_{i,k}$ (Eq. (3.14)) for the ranges $\theta_{\mathrm{CM}} = 30° \dots 150°$ and $E = 1.855 \dots 50.1\,\mathrm{MeV}$.

| $k$ / $,i$ | 1 | 2 | 3 | 4 | 5 | 6 | 7 | 8 | 9 | 10 | 11 | 12 | 13 | 14 | 15 | 16 | 17 | 18 | 19 | 20 | 21 | 22 | 23 | 24 | 25 | 26 | 27 | 28 | 29 |
|---|---|---|---|---|---|---|---|---|---|---|---|---|---|---|---|---|---|---|---|---|---|---|---|---|---|---|---|---|---|
| 1 | 8.78 | 1.78 | -8.70 | -1.44E-02 | -4.04E-02 | 1.38E-01 | 1.22 | -8.29E-01 | -5.68E-06 | 5.82E-02 | 6.52E-03 | -9.04E-04 | 3.23E-05 | -5.02E-07 | 3.12E-09 | -2.00E-01 | 1.30E-01 | -2.02E-03 | 7.02E-05 | -5.03E-07 | 6.36E-09 | 5.44E-04 | 1.06E-02 | 4.38E-02 | -1.65E-01 | 4.07E-03 | -6.71E-03 | 1.53E-01 | -8.10E-01 |
| 2 | 1.78 | 3.40E-01 | -1.74 | -2.59E-03 | -9.09E-03 | 2.31E-02 | 1.18E-01 | -1.42E-01 | -1.55E-06 | 1.14E-02 | 1.57E-03 | -1.85E-04 | 6.43E-06 | -1.00E-07 | 6.28E-10 | -4.04E-02 | 2.65E-02 | -4.15E-04 | 7.12E-06 | 4.09E-08 | 1.28E-09 | -2.09E-04 | 8.90E-04 | 9.05E-03 | -3.41E-02 | 9.03E-04 | -9.47E-04 | -6.41E-02 | -1.34E-01 |
| 3 | -8.70 | -1.74 | 8.62 | 1.39E-02 | 4.55E-02 | -1.26E-01 | -9.25E-01 | 8.04E-01 | 4.94E-06 | -5.80E-02 | -6.77E-03 | 8.98E-04 | -3.18E-05 | 4.95E-07 | -3.09E-09 | 1.99E-01 | -1.30E-01 | 2.05E-03 | -6.15E-05 | 3.22E-07 | -6.30E-09 | -1.64E-04 | -9.08E-03 | -4.37E-02 | 1.65E-01 | -4.53E-03 | 6.02E-03 | 6.88E-02 | 7.78E-01 |
| 4 | -1.44E-02 | -2.59E-03 | 1.39E-02 | 1.84E-05 | 7.05E-05 | -1.63E-04 | -3.14E-04 | 9.28E-04 | 1.86E-08 | -8.62E-05 | -1.46E-05 | 1.52E-06 | -5.14E-08 | 8.03E-10 | -5.06E-12 | 3.24E-04 | -2.14E-04 | 3.30E-06 | 1.76E-09 | -1.47E-09 | -1.03E-11 | 4.27E-06 | 3.01E-06 | -7.45E-05 | 2.81E-04 | -6.98E-06 | 4.55E-06 | 1.00E-03 | 8.26E-04 |
| 5 | -4.04E-02 | -9.09E-03 | 4.55E-02 | 7.05E-05 | 2.51E-03 | 1.08E-03 | 4.68E-02 | 1.05E-02 | -4.57E-07 | -4.63E-04 | -2.91E-05 | 4.38E-06 | -1.59E-07 | 2.53E-09 | -1.61E-11 | 1.19E-03 | -7.75E-04 | 2.01E-05 | -7.40E-07 | 6.74E-09 | -2.99E-11 | -8.14E-05 | -3.72E-04 | -2.45E-04 | 9.10E-04 | -2.23E-04 | -1.99E-05 | 4.08E-02 | 8.11E-03 |
| 6 | 1.38E-01 | 2.31E-02 | -1.26E-01 | -1.63E-04 | 1.08E-03 | -2.34E-02 | -3.95E-01 | 3.00E-02 | 4.80E-06 | 4.19E-04 | 1.93E-04 | -1.89E-05 | 6.79E-07 | -1.12E-08 | 7.23E-11 | -2.43E-03 | 1.58E-03 | -2.13E-05 | -7.04E-07 | 2.31E-08 | 9.38E-11 | -9.90E-05 | -2.73E-04 | 6.86E-04 | -2.59E-03 | -1.04E-04 | 5.75E-04 | -2.48E-01 | 3.87E-02 |
| 7 | 1.22 | 1.18E-01 | -9.25E-01 | -3.14E-04 | 4.68E-02 | -3.95E-01 | -3.46 | 1.10 | 7.09E-05 | -2.67E-03 | 2.66E-03 | -1.73E-04 | 5.39E-06 | -8.58E-08 | 5.41E-10 | -1.39E-02 | 9.43E-03 | 1.20E-05 | -3.79E-05 | 7.44E-07 | 7.76E-10 | -3.14E-03 | -1.15E-02 | 6.02E-03 | -2.31E-02 | -4.29E-03 | 1.04E-02 | -9.18E-01 | 9.79E-01 |
| 8 | -8.29E-01 | -1.42E-01 | 8.04E-01 | 9.28E-04 | 1.05E-02 | 3.00E-02 | 1.10 | 2.46E-01 | -1.07E-05 | -4.94E-03 | -1.07E-03 | 1.04E-04 | -3.72E-06 | 6.33E-08 | -4.24E-10 | 1.86E-02 | -1.24E-02 | 2.23E-04 | 2.89E-06 | -1.47E-07 | -5.80E-10 | 1.27E-04 | -2.92E-04 | -4.44E-03 | 1.67E-02 | -1.01E-03 | -8.88E-04 | 1.08 | 1.87E-01 |
| 9 | -5.68E-06 | -1.55E-06 | 4.94E-06 | 1.86E-08 | -4.57E-07 | 4.80E-06 | 7.09E-05 | -1.07E-05 | -5.97E-10 | 3.40E-08 | -4.77E-09 | 1.27E-09 | -5.45E-11 | 8.98E-13 | -5.56E-15 | -9.81E-09 | 2.06E-08 | -1.49E-09 | -1.76E-10 | 3.89E-12 | -3.66E-15 | 4.70E-09 | 1.61E-08 | -1.54E-08 | 5.95E-08 | 4.56E-08 | -1.94E-07 | 4.41E-05 | -1.32E-05 |
| 10 | 5.82E-02 | 1.14E-02 | -5.80E-02 | -8.62E-05 | -4.63E-04 | 4.19E-04 | -2.67E-03 | -4.94E-03 | 3.40E-08 | 7.76E-04 | -1.68E-05 | -2.84E-07 | -3.11E-08 | 1.44E-09 | -1.37E-11 | -2.26E-03 | 1.65E-03 | -1.53E-05 | 3.35E-07 | -8.79E-11 | 4.66E-11 | -2.29E-05 | -2.76E-05 | 3.00E-04 | -1.14E-03 | 4.50E-05 | -2.34E-05 | -6.95E-03 | -4.60E-03 |
| 11 | 6.52E-03 | 1.57E-03 | -6.77E-03 | -1.46E-05 | -2.91E-05 | 1.93E-04 | 2.66E-03 | -1.07E-03 | -4.77E-09 | -1.68E-05 | 1.43E-05 | -1.73E-06 | 7.14E-08 | -1.30E-09 | 9.01E-12 | 6.91E-06 | -3.60E-05 | -1.49E-06 | 1.33E-07 | -1.97E-09 | 4.02E-12 | 6.88E-06 | 3.25E-05 | 3.01E-05 | -1.12E-04 | 2.97E-06 | -1.08E-05 | 1.28E-03 | -1.10E-03 |
| 12 | -9.04E-04 | -1.85E-04 | 8.98E-04 | 1.52E-06 | 4.38E-06 | -1.89E-05 | -1.73E-04 | 1.04E-04 | 1.27E-09 | -2.84E-07 | -1.73E-06 | 1.90E-07 | -7.51E-09 | 1.35E-10 | -9.32E-13 | 7.10E-06 | -2.24E-06 | 2.07E-07 | -7.52E-09 | 5.73E-11 | -5.83E-13 | -2.80E-07 | -1.89E-06 | -4.44E-06 | 1.66E-05 | -4.39E-07 | 8.52E-07 | -3.57E-05 | 1.01E-04 |
| 13 | 3.23E-05 | 6.43E-06 | -3.18E-05 | -5.14E-08 | -1.59E-07 | 6.79E-07 | 5.39E-06 | -3.72E-06 | -5.45E-11 | -3.11E-08 | 7.14E-08 | -7.51E-09 | 3.00E-10 | -5.47E-12 | 3.83E-14 | -1.73E-07 | 1.91E-08 | -7.33E-09 | 2.00E-10 | -7.14E-13 | 2.03E-14 | 7.46E-09 | 5.69E-08 | 1.59E-07 | -5.97E-07 | 1.59E-08 | -2.77E-08 | 4.12E-07 | -3.57E-06 |
| 14 | -5.02E-07 | -1.00E-07 | 4.95E-07 | 8.03E-10 | 2.53E-09 | -1.12E-08 | -8.58E-08 | 6.33E-08 | 8.98E-13 | 1.44E-09 | -1.30E-09 | 1.35E-10 | -5.47E-12 | 1.02E-13 | -7.22E-16 | 5.35E-10 | 1.42E-09 | 1.13E-10 | -3.08E-12 | 1.08E-14 | -3.02E-16 | -1.37E-10 | -9.56E-10 | -2.46E-09 | 9.21E-09 | -2.53E-10 | 4.49E-10 | -3.01E-09 | 6.06E-08 |
| 15 | 3.12E-09 | 6.28E-10 | -3.09E-09 | -5.06E-12 | -1.61E-11 | 7.23E-11 | 5.41E-10 | -4.24E-10 | -5.56E-15 | -1.37E-11 | 9.01E-12 | -9.32E-13 | 3.83E-14 | -7.22E-16 | 5.16E-18 | 7.39E-12 | -1.74E-11 | -7.06E-13 | 1.98E-14 | -8.14E-17 | 1.82E-18 | 9.94E-13 | 6.43E-12 | 1.53E-11 | -5.69E-11 | 1.61E-12 | -2.90E-12 | 1.23E-12 | -4.06E-10 |
| 16 | -2.00E-01 | -4.04E-02 | 1.99E-01 | 3.24E-04 | 1.19E-03 | -2.43E-03 | -1.39E-02 | 1.86E-02 | -9.81E-09 | -2.26E-03 | 6.91E-06 | 7.10E-06 | -1.73E-07 | 5.35E-10 | 7.39E-12 | 6.78E-03 | -4.85E-03 | 4.87E-05 | -1.63E-06 | 1.11E-08 | -1.56E-10 | 5.04E-05 | -7.52E-06 | -1.00E-03 | 3.79E-03 | 6.87E-08 | 1.30E-04 | 6.88E-03 | 1.80E-02 |
| 17 | 1.30E-01 | 2.65E-02 | -1.30E-01 | -2.14E-04 | -7.75E-04 | 1.58E-03 | 9.43E-03 | -1.24E-02 | 2.06E-08 | 1.65E-03 | -3.60E-05 | -2.24E-06 | 1.91E-08 | 1.42E-09 | -1.74E-11 | -4.85E-03 | 3.54E-03 | -3.16E-05 | 1.14E-06 | -8.80E-09 | 1.03E-10 | -5.18E-05 | -6.89E-05 | 6.44E-04 | -2.44E-03 | 7.72E-05 | -8.72E-05 | -4.27E-03 | -1.20E-02 |
| 18 | -2.02E-03 | -4.15E-04 | 2.05E-03 | 3.30E-06 | 2.01E-05 | -2.13E-05 | 1.20E-05 | 2.23E-04 | -1.49E-09 | -1.53E-05 | -1.49E-06 | 2.07E-07 | -7.33E-09 | 1.13E-10 | -7.06E-13 | 4.87E-05 | -3.16E-05 | 3.19E-05 | -4.46E-06 | 7.94E-08 | -1.69E-12 | 1.88E-04 | 2.32E-03 | -3.86E-04 | 1.43E-03 | -1.93E-06 | 1.28E-06 | 1.96E-04 | 2.13E-04 |
| 19 | 7.02E-05 | 7.12E-06 | -6.15E-05 | 1.76E-09 | -7.40E-07 | -7.04E-07 | -3.79E-05 | 2.89E-06 | -1.76E-10 | 3.35E-07 | 1.33E-07 | -7.52E-09 | 2.00E-10 | -3.08E-12 | 1.98E-14 | -1.63E-06 | 1.14E-06 | -4.46E-06 | 9.20E-07 | -1.74E-08 | 9.74E-14 | -5.97E-05 | -3.53E-04 | 4.54E-05 | -1.64E-04 | 6.87E-08 | 9.19E-08 | -3.26E-05 | 4.61E-06 |
| 20 | -5.03E-07 | 4.09E-08 | 3.22E-07 | -1.47E-09 | 6.74E-09 | 2.31E-08 | 7.44E-07 | -1.47E-07 | 3.89E-12 | -8.79E-11 | -1.97E-09 | 5.73E-11 | -7.14E-13 | 1.08E-14 | -8.14E-17 | 1.11E-08 | -8.80E-09 | 7.94E-08 | -1.74E-08 | 3.46E-10 | -1.24E-15 | 1.16E-06 | 6.33E-06 | -7.80E-07 | 2.81E-06 | -5.98E-10 | -2.44E-09 | 5.73E-07 | -1.78E-07 |
| 21 | 6.36E-09 | 1.28E-09 | -6.30E-09 | -1.03E-11 | -2.99E-11 | 9.38E-11 | 7.76E-10 | -5.80E-10 | -3.66E-15 | 4.66E-11 | 4.02E-12 | -5.83E-13 | 2.03E-14 | -3.02E-16 | 1.82E-18 | -1.56E-10 | 1.03E-10 | -1.69E-12 | 9.74E-14 | -1.24E-15 | 1.31E-13 | -1.76E-11 | -1.52E-03 | 3.09E-11 | -1.16E-10 | 3.00E-12 | -4.56E-12 | 3.63E-11 | -5.65E-10 |
| 22 | 5.44E-04 | -2.09E-04 | -1.64E-04 | 4.27E-06 | -8.14E-05 | -9.90E-05 | -3.14E-03 | 1.27E-04 | 4.70E-09 | -2.29E-05 | 6.88E-06 | -2.80E-07 | 7.46E-09 | -1.37E-10 | 9.94E-13 | 5.04E-05 | -5.18E-05 | 1.88E-04 | -5.97E-05 | 1.16E-06 | -1.76E-11 | 2.16E-02 | 7.13E-02 | 7.43E-03 | -1.75E-02 | 7.22E-06 | 6.95E-06 | -2.49E-03 | 2.61E-04 |
| 23 | 1.06E-02 | 8.90E-04 | -9.08E-03 | 3.01E-06 | -3.72E-04 | -2.73E-04 | -1.15E-02 | -2.92E-04 | 1.61E-08 | -2.76E-05 | 3.25E-05 | -1.89E-06 | 5.69E-08 | -9.56E-10 | 6.43E-12 | -7.52E-06 | -6.89E-05 | 2.32E-03 | -3.53E-04 | 6.33E-06 | -1.52E-03 | 7.13E-02 | 1.04E-01 | 3.50E-02 | -2.97E-02 | 3.35E-05 | 2.15E-05 | -9.83E-03 | 2.56E-04 |
| 24 | 4.38E-02 | 9.05E-03 | -4.37E-02 | -7.45E-05 | -2.45E-04 | 6.86E-04 | 6.02E-03 | -4.44E-03 | -1.54E-08 | 3.00E-04 | 3.01E-05 | -4.44E-06 | 1.59E-07 | -2.46E-09 | 1.53E-11 | -1.00E-03 | 6.44E-04 | -3.86E-04 | 4.54E-05 | -7.80E-07 | 3.09E-11 | 7.43E-03 | 3.50E-02 | 1.81E-03 | -2.04E-02 | 2.43E-05 | -3.57E-05 | 6.72E-04 | -4.35E-03 |
| 25 | -1.65E-01 | -3.41E-02 | 1.65E-01 | 2.81E-04 | 9.10E-04 | -2.59E-03 | -2.31E-02 | 1.67E-02 | 5.95E-08 | -1.14E-03 | -1.12E-04 | 1.66E-05 | -5.97E-07 | 9.21E-09 | -5.69E-11 | 3.79E-03 | -2.44E-03 | 1.43E-03 | -1.64E-04 | 2.81E-06 | -1.16E-10 | -1.75E-02 | -2.97E-02 | -2.04E-02 | 9.21E-02 | -9.02E-05 | 1.35E-04 | -2.89E-03 | 1.64E-02 |
| 26 | 4.07E-03 | 9.03E-04 | -4.53E-03 | -6.98E-06 | -2.23E-04 | -1.04E-04 | -4.29E-03 | -1.01E-03 | 4.56E-08 | 4.50E-05 | 2.97E-06 | -4.39E-07 | 1.59E-08 | -2.53E-10 | 1.61E-12 | 6.87E-08 | 7.72E-05 | -1.93E-06 | 6.87E-08 | -5.98E-10 | 3.00E-12 | 7.22E-06 | 3.35E-05 | 2.43E-05 | -9.02E-05 | 1.99E-05 | 1.28E-06 | -3.75E-03 | -8.29E-04 |
| 27 | -6.71E-03 | -9.47E-04 | 6.02E-03 | 4.55E-06 | -1.99E-05 | 5.75E-04 | 1.04E-02 | -8.88E-04 | -1.94E-07 | -2.34E-05 | -1.08E-05 | 8.52E-07 | -2.77E-08 | 4.49E-10 | -2.90E-12 | 1.30E-04 | -8.72E-05 | 1.28E-06 | 9.19E-08 | -2.44E-09 | -4.56E-12 | 6.95E-06 | 2.15E-05 | -3.57E-05 | 1.35E-04 | 1.28E-06 | 8.69E-06 | 4.75E-03 | -6.21E-04 |
| 28 | 1.53E-01 | -6.41E-02 | 6.88E-02 | 1.00E-03 | 4.08E-02 | -2.48E-01 | -9.18E-01 | 1.08 | 4.41E-05 | -6.95E-03 | 1.28E-03 | -3.57E-05 | 4.12E-07 | -3.01E-09 | 1.23E-12 | 6.88E-03 | -4.27E-03 | 1.96E-04 | -3.26E-05 | 5.73E-07 | 3.63E-11 | -2.49E-03 | -9.83E-03 | 6.72E-04 | -2.89E-03 | -3.75E-03 | 4.75E-03 | 1.04 | 8.53E-01 |
| 29 | -8.10E-01 | -1.34E-01 | 7.78E-01 | 8.26E-04 | 8.11E-03 | 3.87E-02 | 9.79E-01 | 1.87E-01 | -1.32E-05 | -4.60E-03 | -1.10E-03 | 1.01E-04 | -3.57E-06 | 6.06E-08 | -4.06E-10 | 1.80E-02 | -1.20E-02 | 2.13E-04 | 4.61E-06 | -1.78E-07 | -5.65E-10 | 2.61E-04 | 2.56E-04 | -4.35E-03 | 1.64E-02 | -8.29E-04 | -6.21E-04 | 8.53E-01 | 1.69E-01 |

# List of Figures

# List of Tables

# Bibliography

[1] P. Reichart, G. Datzmann, A. Hauptner, R. Hertenberger, C. Wild, G. Dollinger, Three-dimensional hydrogen microscopy in diamond, Science (306) (2004) 1537–1540.

[2] P. Reichart, G. Dollinger, Hydrogen analysis by proton proton scattering, in: Y. Wang, M. Nastasi (Eds.), Handbook of Modern Ion Beam Material Analysis, 2nd Edition, Materials Research Society, 2009.

[3] J. R. Bergervoet, P. C. van Campen, W. A. van der Sanden, J. J. de Swart, Phase shift analysis of 0-30 MeV pp scattering data, Phys. Rev. C 38 (1) (1988) 15–50. `doi:10.1103/PhysRevC.38.15`.

[4] J. R. Bergervoet, P. C. van Campen, R. A. M. Klomp, J.-L. de Kok, T. A. Rijken, V. G. J. Stoks, J. J. de Swart, Phase shift analysis of all proton-proton scattering data below $T_{lab}$=350 MeV, Phys. Rev. C 41 (4) (1990) 1435–1452. `doi:10.1103/PhysRevC.41.1435`.

[5] M. H. MacGregor, R. A. Arndt, R. M. Wright, Determination of the nucleon-nucleon scattering matrix. x. $(p,p)$ and $(n,p)$ analysis from 1 to 450 MeV, Phys. Rev. 182 (5) (1969) 1714–1728. `doi:10.1103/PhysRev.182.1714`.

[6] C. J. Joachain, Quantum collision theory, Elsevier Science Publishing Company, 1984.

[7] J. M. Blatt, V. F. Weisskopf, Theor. Nucl. Phys., new Edition, Dover Publications Inc., April 1991.

[8] N. F. Mott, The collision between two electrons, Proc. R. Soc. London, Ser. A 126 (801) (1930) 259–267.

[9] G. Breit, E. U. Condon, R. D. Present, Theory of scattering of protons by protons, Phys. Rev. 50 (9) (1936) 825–845. `doi:10.1103/PhysRev.50.825`.

[10] D. J. Knecht, P. F. Dahl, S. Messelt, Proton-proton scattering: Revision and analysis of experimental measurements from 1.4 to 3.0 MeV, Phys. Rev. 148 (3) (1966) 1031–1044.

[11] J. Bystricky, F. Lehar, et al., Numerical data and functional relationships in science and technology, in: K.-H. Hellwege, H. Schopper (Eds.), Elastic and Charge Exchange Scattering of Elementary Particles, Vol. 9a of Landolt–Börnstein (New Series – Group I), Springer, Berlin, 1980, p. 110 ff.

[12] IAEA Nucl. Data Services, int. Atomic Energy Agency, Austria, www-nds.iaea.org (2009).

[13] NNDC Databases, brookhaven National Laboratory, USA, www.nndc.bnl.gov (2009).

[14] M. Chadwick, P. G. Young, G. M. Hale, Dla150 documentation of cross sections, heating, and damage, Los Alamos National Laboratory Report LA-UR-99-1222.

[15] H. R. Worthington, J. N. McGruer, D. E. Findley, Proton-proton scattering from 1.8 MeV to 4.2 MeV, Phys. Rev. 90 (5) (1953) 899.

[16] K. Imai, K. Nisimura, N. Tamura, H. Sato, Measurements of proton-proton differential cross sections at 5, 7 and 8 MeV, Nucl. Phys. A 246 (1) (1975) 76–92.

[17] R. J. Slobodrian, H. E. Conzett, E. Shield, W. F. Tivol, Proton-proton elastic scattering between 6 and 10 MeV, Phys. Rev. 174 (4) (1968) 1122.

[18] N. Jarmie, J. H. Jett, J. L. Detch, R. L. Hutson, Proton-proton scattering at 9.690, 9.918, and 13.600 MeV, Phys. Rev. Lett. 25 (1) (1970) 34.

[19] S. Kikuchi, J. Sanada, S. Suwa, I. Hayashi, K. Nisimura, K. Fukunaga, Elastic scattering of 14 MeV protons by deuterons and by protons, J. Phys. Soc. Jpn. 15 (1) (1960) 9–17.

[20] J. L. Yntema, M. G. White, Scattering of protons by hydrogen near 18 MeV, Phys. Rev. 95 (5) (1954) 1226.

[21] J. W. Burkig, J. R. Richardson, G. E. Schrank, Proton-proton scattering at 19.8 MeV, Phys. Rev. 113 (1) (1959) 290.

[22] T. H. Jeong, L. H. Johnston, D. E. Young, C. N. Waddell, Proton-proton scattering at 25 MeV, Phys. Rev. 118 (4) (1960) 1080.

[23] W. K. H. Panofsky, F. L. Fillmore, The scattering of protons by protons near 30 MeV, photographic method, Phys. Rev. 79 (1) (1950) 57.

[24] F. L. Fillmore, Proton-proton scattering near 30 MeV, Phys. Rev. 83 (1951) 1252.

[25] L. H. Johnston, D. A. Swenson, Proton-proton scattering at 40 MeV, Phys. Rev. 111 (1) (1958) 212.

[26] A. Berdoz, F. Foroughi, C. Nussbaum, The differential cross section of elastic proton-proton scattering at 50 MeV, J. Phys. G 12 (6) (1986) L133–L137.

[27] IAEA Nucl. Data Services, int. Atomic Energy Agency, Austria, www-nds.iaea.org, manual for data evaluation. (2010).

[28] IAEA Nucl. Data Services, int. Atomic Energy Agency, Austria, http://www-nds.iaea.org/sigmacalc/ (2010).

[29] M. Moser, P. Reichart, C. Greubel, G. Dollinger, tabulated Proton-Proton Scattering Cross Sections, Munich, www.e12.physik.tu-muenchen.de/groups/rim/pp or alternatively www.unibw.de/lrt2/forschung-en/snake/pp (2010).

# Danksagung

Als erstes möchte ich mich bei Herrn Professor Dr. Sotier für die freundliche Übernahme der Masterarbeit und die zahlreichen Hilfestellungen in formalen Dingen bedanken. Ebenso möchte ich mich bei Herrn Professor Günther Dollinger für das Angebot der Masterarbeit und die nette Aufnahme in seinen Lehrstuhl bedanken. Besonders beeindruckt war ich von dem ständigen offenen Ohr seinerseits für Probleme die ich während der Erstellung dieser Arbeit hatte und die zahlreichen äusserst fruchtbaren und ausführlichen Diskussionen.

Bei meinem Betreuer Herrn Dr. Patrick Reichart möchte ich mich bedanke für das große Vertrauen, die viele Zeit, die vielen aufschlussreichen Diskussionen und sein Engagement, dass er mir entgegengebracht hat und die interessante Themenstellung meiner Masterarbeit.

Bei Herrn Christoph Greubel möchte ich mich auch für die vielen Tipps und Diskussion in Problemen und offenen Fragestellungen während der Erstellung dieser Arbeit bedanken.

Allen Mitgliedern der Snake-Gruppe möchte ich für die nette Aufnahme in Ihr Team sowie die Unterstützung und die angenehme Arbeitsatmosphäre danken.

Meinem Bruder Michael und meinen Freunden möchte ich für die Geduld während meiner Masterarbeit danken. Auch wenn ich sie manchmal zeitlich vernachlässigt habe, hatten sie für meine Situation immer Verständnis.

Meiner Freundin Daniela danke ich, für all die Ausdauer, das Verständnis und den Rückhalt den sie mir gab während des Studiums und besonders bei der

Anfertigung dieser Arbeit.

Meinen lieben Eltern, Traute und Fritz Moser, danke ich besonders für die großartige Unterstützung den Rückhalt und das Vertrauen, welches ich während meiner gesamten Studienzeit sowie der Masterarbeit, immer sicher war und bin.

# Danke!

| Name: | Marcus Moser |
|---|---|
| Geb.: | 05.01.1983 |
| Matr.Nr.: | 29450304 |
| Sudiengruppe: | 3; Mikro- und Nanotechnik (Master) |
| Semester | WS 10/11 |

# Erklärung

gemäß § 13 Abs. 5 RaPO

Hiermit erkläre ich, dass ich die Masterarbeit selbstständig verfasst, noch nicht anderweitig für Prüfungszwecke vorgelegt, keine anderen als die angegebenen Quellen oder Hilfsmittel benützt sowie wörtliche und sinngemäße Zitate als solche gekennzeichnet habe.

_____          _____

Ort, Datum                                      Unterschrift